Differential GTP-dependent *in-vitro* polymerization of recombinant Physcomitrella FtsZ proteins

Stella W. L. Milferstaedt[1,3], Marie Joest[2], Sebastian N. W. Hoernstein[1], Lennard L. Bohlender[1], Buğra Özdemir[1,5], Chris van der Does[2], Eva L. Decker[1], Ralf Reski[1,3,4,*]

[1]Plant Biotechnology, Faculty of Biology, University of Freiburg, Schaenzlestr. 1, 79104 Freiburg, Germany

[2]Molecular Biology of Archaea, Faculty of Biology, University of Freiburg, Schaenzlestr. 1, 79104 Freiburg, Germany

[3]Cluster of Excellence *liv*MatS @ FIT – Freiburg Centre for Interactive Materials and Bioinspired Technologies, University of Freiburg, Georges-Köhler-Allee 105, 79110 Freiburg, Germany

[4]Signalling Research Centres BIOSS and CIBSS, Schaenzlestr. 18, 79104 Freiburg, Germany

[5]Present address: Euro-BioImaging Bio-Hub, EMBL, Meyerhofstraße 1, 69117 Heidelberg, Germany

ORCID IDs:

S.W.L.M. 0000-0003-3357-4177

M.J. 0009-0004-4997-505X

S.N.W.H. 0000-0002-2095-689X

L.L.B. 0000-0002-4599-7807

B.Ö. 0000-0001-9823-0581

C.v.d.D. 0000-0002-7348-7361

E.L.D. 0000-0002-9151-1361

R.R. 0000-0002-5496-6711

*Corresponding author: ralf.reski@biologie.uni-freiburg.de

1. Abstract

Cell division in bacteria and plastid division in plants both require self-assembling Filamentous temperature-sensitive Z (FtsZ) proteins as key components of their division machinery. FtsZ proteins are soluble GTPases sharing structural and biochemical similarities with eukaryotic tubulin. In the moss Physcomitrella, the morphology of the FtsZ polymer networks varies between the different FtsZ isoforms. The underlying mechanism and foundation of the distinct networks is unknown. Here, we investigated the interaction of Physcomitrella FtsZ2-1 with FtsZ1 isoforms *via* co-immunoprecipitation and mass spectrometry, and found protein-protein interaction *in vivo*. We tagged FtsZ1-2 and FtsZ2-1 with different fluorophores and expressed both in *E. coli*, which led to the formation of defined structures within the cells and to an influence on bacterial cell division. Furthermore, we have optimized the purification protocols for FtsZ1-2 and FtsZ2-1 from *E. coli* and characterized their GTPase activity and polymerization *in vitro*. Both FtsZ isoforms showed GTPase activity, a prerequisite for polymerization. In light scattering assays, we observed GTP-dependent assembly of FtsZ1-2, but not of FtsZ2-1. In contrast, transmission electron microscopy demonstrated GTP-dependent filament formation of both isoforms. Taken together, our results reveal that Physcomitrella FtsZ1-2 and FtsZ2-1 are functionally different and that both isoforms differ in their properties from FtsZ proteins from bacteria, archaea and vascular plants.

Keywords: cytoskeleton, FtsZ polymerization, GTPase, plastoskeleton, self-assembly

2. Introduction

Plants harvest energy from oxygenic photosynthesis, during which light is the energy source for the fixation of atmospheric CO_2 in organic compounds, while O_2 is produced as a side product. In eukaryotic cells, photosynthesis depends on chloroplasts (Leister, 2019). These cell organelles derived from endosymbiosis, where a eukaryote engulfed a free-living, photoautotrophic cyanobacterial-like prokaryote (Gould et al., 2008; Keeling, 2013; Zimorski et al., 2014). While some genes of prokaryotic origin disappeared over time, or were retained in the organellar genome, respectively, most were transferred to the host nucleus after the endosymbiotic event (Martin et al., 1998). The relation of these organelles to prokaryotes explains why chloroplasts do not develop *de novo* but divide by binary fission (McFadden, 1999), while at the same time suggesting that prokaryotic cytokinesis and cell organelle division are conserved mechanisms (Osteryoung & Vierling, 1995; Strepp et al., 1998).

Most bacteria and chloroplasts of bryophytes, comprising mosses, liverworts, and hornworts, are surrounded by a peptidoglycan wall (Silhavy et al., 2010; Hirano et al., 2016; MacLeod et al., 2023), which needs to be remodelled during bacterial cell division (Bisson Filho et al., 2017; Barrows and Goley, 2021). Proteins involved in bacterial cell division are also responsible for plastid division in plants (Strepp et al., 1998; McFadden, 1999). Both mechanisms require Filamentous temperature-sensitive Z (FtsZ) proteins as a key component of the division machinery (Dai and Lutkenhaus, 1991; Osteryoung et al., 1998). FtsZ proteins were named after one of the filamentous temperature-sensitive *Escherichia coli* (*E. coli*) mutants, which grows filamentous due to their inability to divide at elevated temperatures (Lutkenhaus et al., 1980). FtsZ proteins assemble into a ring structure, the Z-ring, thus determining the future division site of bacteria and chloroplasts (Bi & Lutkenhaus, 1991; Vitha et al., 2001; Yoshida et al., 2016). In *E. coli* and *Bacillus subtilis*, FtsZ-function is coupled to peptidoglycan synthesis (Bisson-Filho et al., 2017; Yang et al., 2017). Remarkably, bacterial cell division as well as division of moss chloroplasts, but not plastid division of vascular plants, is sensitive to beta-lactam antibiotics (Kasten & Reski, 1997).

FtsZ proteins are soluble guanosine triphosphatases (GTPases) (de Boer et al., 1992; Smith et al., 2010; Porter et al., 2021) that share structural and biochemical similarities with the eukaryotic cytoskeletal protein tubulin (Erickson, 1995; Santana-Molina et al., 2023). FtsZ proteins have similar functions in bacteria and plastids (Osteryoung & Vierling, 1995; Strepp et al., 1998). The nuclear-encoded plant FtsZ proteins are imported into the chloroplast (Osteryoung & Vierling, 1995), where they are required for plastid division as well as plastid shaping (Kiessling et al., 2000). In most bacteria, FtsZ is encoded by a single gene (Lutkenhaus & Addinall, 1997; Osteryoung & Nunnari, 2003), while archaea (Santana-Molina et al., 2023) and plants encode predominantly two FtsZ isoforms. For instance, *Arabidopsis thaliana* (Arabidopsis) encodes FtsZ1 and FtsZ2 (Osteryoung & Vierling, 1995; Osteryoung et al., 1998). These arose from a gene duplication (Rensing et al., 2004), in which plant FtsZ1 arose from FtsZ2 (Miyagishima et al., 2004; TerBush et al., 2013).

In the vascular plant Arabidopsis, both FtsZ isoforms have non-redundant functions since their independent expression inhibition led in both cases to a reduced number of chloroplasts (Osteryoung et al., 1998). The rings formed by Arabidopsis FtsZ1 and FtsZ2 colocalize *in vivo* at the chloroplast centre (Vitha et al., 2001) and form heteropolymers at the future division site upon recombinant expression in the yeast *Pichia pastoris* (new species name *Komagataella phaffii*) (Yoshida et al., 2016). Also, the polymerization behaviour of Arabidopsis FtsZ isoforms has been characterized *in vitro* (Olson et al., 2010; Porter et al., 2021). Here, FtsZ1 and FtsZ2 show differences in their GTPase activity and polymerization mechanism and only FtsZ2 polymerized on its own (Porter et al., 2021).

Furthermore, FtsZ1 and FtsZ2 show differences regarding their protein structure. In general, FtsZ proteins contain two domains, a widely conserved N-terminal GTPase domain and a C-terminal region (Löwe & Amos, 1998; TerBush et al., 2013). The GTPase domain comprises a GTP-binding domain and a GTPase-activating domain. Together, they represent the core structure of FtsZ (Yoshida et al., 2016), since the C-terminal region is more variable (Osteryoung & McAndrew, 2001). The N-terminal domain is responsible for GTP binding and hydrolysis (Löwe & Amos, 1998). FtsZ2 proteins contain an additional short motif at the C-terminus that is missing in FtsZ1 (Miyagishima et al., 2004; TerBush et al., 2013). In Arabidopsis, this motif is responsible for the interaction of FtsZ2 with transmembrane proteins (TerBush et al., 2013). Recently, a conserved sequence motif of the C-terminal domain of Arabidopsis FtsZ1 was identified that is involved in membrane binding and interactions with other proteins of the plastid division machinery (Liu et al., 2022). Moreover, the N- as well as the C-terminus of both isoforms are involved in polymer formation of FtsZ1 and FtsZ2 (TerBush et al., 2016).

The moss Physcomitrella (new species name *Physcomitrium patens*) encodes the uniquely high number of five different FtsZ proteins (FtsZ1-1, FtsZ1-2, FtsZ2-1, FtsZ2-2, FtsZ3), which fall in three clades (FtsZ1, FtsZ2, FtsZ3), indicating neofunctionalisation of the different isoforms during evolution (Rensing et al., 2004; Martin et al., 2009a; Grosche & Rensing, 2017). Arabidopsis FtsZ1 and FtsZ2 are orthologues to Physcomitrella FtsZ1 and FtsZ2 (Martin et al., 2009a; Grosche & Rensing, 2017). Among those FtsZ isoforms, FtsZ2-1 was proven to be involved in chloroplast division (Strepp et al., 1998; Khraiwesh et al., 2008; Martin et al., 2009b).

The Physcomitrella FtsZ proteins assemble in network-like structures inside the chloroplast (Kiessling et al., 2000; Suppanz et al., 2007). Using reverse genetics, the diverse and non-redundant functions of the five FtsZ isoforms in Physcomitrella were investigated (Martin et al., 2009b). Here, the analysis of distinct single and double knockout mutants of Physcomitrella *ftsZ* genes revealed their roles in chloroplast division, chloroplast shaping, as well as their network assembling properties within the chloroplast (Kiessling et al., 2000; Martin et al., 2009b). Due to these characteristics, the Physcomitrella FtsZ proteins ensure plastid stability and structural integrity (Kiessling et al., 2000; Reski, 2009). Since this FtsZ network in moss plastids resembles the structure of the eukaryotic cytoskeleton, the term ‘plastoskeleton’ was coined to describe its organization and function in plastids (Kiessling et al., 2000; Reski, 2002). Subsequently, it was discovered that not only eukaryotes but also bacteria have a highly

dynamic cytoskeleton and that FtsZ is a part of it (Shih & Rothfield, 2006; Erickson et al., 2010; Loose & Mitchison, 2014; Wagstaff & Löwe, 2018).

Unlike described for other plants, proteins of the nuclear *ftsZ* genes are not only imported into plastids but are dually targeted to chloroplasts and the cytosol in Physcomitrella, suggesting that they also have functions beyond plastid division (Kiessling et al., 2004). Interestingly, this coincides with a low diversification of the cytoskeletal protein family tubulin in Physcomitrella (Jost et al., 2005). Subsequently, Physcomitrella FtsZ proteins were found to be involved in cell patterning, plant development, and gravity sensing (Martin et al., 2009b). Additionally, distinct localization-dependent *in-vivo* interactions among four of the five Physcomitrella FtsZ isoforms were revealed by using fluorescence resonance energy transfer (FRET) (Gremillon et al., 2007).

The morphology of the Physcomitrella FtsZ polymer networks varies between the different isoforms. *In-vivo* network analysis using GFP-tagged FtsZ1-2 and FtsZ2-1 indicated functional differences between them (Özdemir et al., 2018). While the FtsZ2-1 network is exclusively formed within the chloroplast, FtsZ1-2 networks form long, extra-plastidic extensions and may play a role in the formation of stromules (Özdemir et al., 2018), stroma-filled, tubular connections between chloroplasts (Köhler et al., 1997). The FtsZ1-2 network also contains significantly more nodes than the FtsZ2-1 network, while so-called meganodes (extraordinarily large nodes) occur only with FtsZ2-1. Moreover, the FtsZ2-1 filaments are more curved *in vivo*, thicker in segment size and resemble the microtubules of the cytoskeleton more than FtsZ1-2. Thus, this resemblance hints towards mechanical properties that might be interesting when using Physcomitrella FtsZ filaments to develop sustainable material systems (Asgharzadeh et al., 2020). Based on the identified morphological differences of Physcomitrella FtsZ1-2 and FtsZ2-1 (Özdemir et al., 2018), the mechanical behaviour and load-bearing responses of the two Physcomitrella FtsZ isoforms were investigated in *in-silico* experiments, relating the structure to the function of the FtsZ protein networks (Asgharzadeh et al., 2018; Asgharzadeh et al., 2020; Özdemir & Reski, 2021). The capability of the plastoskeleton to maintain its load-bearing structure even under distortion is based on its material properties as polymers and more importantly, on the structural features of the network (Asgharzadeh et al., 2020).

Besides the mechanical properties of the FtsZ isoforms, knowledge about the polymer-forming properties of Physcomitrella FtsZ proteins as a GTP-driven structure is of particular interest. Combining the data about the load-bearing structure of the plastoskeleton with knowledge about the biochemical foundations could pave the way for adaptive biomimetic materials (Betz et al., 2016; te Brinke et al., 2018) or 3D-printed biopolymer materials for tissue engineering (Kalyan & Kumar, 2022). In various tissues, Physcomitrella FtsZ1-2 and FtsZ2-1 have relatively high expression levels, suggesting division-independent, stable networks within the chloroplast (Özdemir et al., 2018). Therefore, we examined GTPase activity, polymer assembly, and formation of the Physcomitrella FtsZ network *in vitro*. We expressed Physcomitrella FtsZ1-2 and FtsZ2-1 in *E. coli*, purified the proteins, and analysed their GTP-dependent polymerization individually and together. Furthermore, we investigated

the interaction of these isoforms *in vivo*, and visualised both FtsZ isoforms in *E. coli* cells individually and in combination without potential interaction partners.

Different bacterial FtsZ (e.g., *B. subtilis* FtsZ and *E. coli* FtsZ, Król & Scheffers, 2013; *Agrobacterium tumefaciens* FtsZ, Howell et al., 2019; *Synechococcus elongatus*, Porter et al., 2023), archaeal FtsZ (*Haloferax volcanii*; Liao et al., 2021; Ithurbide et al., 2022), and plant FtsZ (Arabidopsis, Porter et al., 2021; Porter et al., 2023) were already investigated regarding their assembly and biochemical properties. Here, we provide insights into the GTP-dependent polymerization and the assembly properties of FtsZ1-2 and FtsZ2-1 of the moss Physcomitrella.

3. Results

3.1. *In-vivo* interaction of Physcomitrella FtsZ2-1 with FtsZ1

Distinct localization-dependent interactions among four of the five Physcomitrella FtsZ isoforms have been revealed by overexpression as GFP fusions (Gremillon et al., 2007). Here, we independently reassessed these results on a physiological level with special focus on the interactions between FtsZ1 isoforms and FtsZ2-1.

To address this, an in-frame fusion of Physcomitrella FtsZ2-1 with GFP at the endogenous locus was generated *via* targeted knock-in (Supplemental Table S1), employing the highly efficient homologous recombination in this moss (Hohe et al., 2004; Wiedemann et al., 2018). Twenty-one selected lines were screened by PCR and from eight positive candidate lines three were chosen for a test immuno-precipitation (IP, Supplemental Figure S1). From those, line #513 was chosen for quantitative Co-immunoprecipitations (Co-IP) performed using GFP-Trap Magnetic Particles as described in Hoernstein et al. (2023), with Physcomitrella wild type (WT) as a negative control. Label-free quantitation values (LFQ) obtained from a *MaxQuant* search (Cox and Mann, 2008; Cox et al., 2014) were used and significant interacting partners were identified at a false discovery rate (FDR) of 0.01 % (Figure 1). The significant interacting proteins can be found in Supplemental Table S2.

From this, Physcomitrella FtsZ1 isoforms were identified as significant interactors of FtsZ2-1 (Figure 1). Thus, we confirmed that FtsZ2-1 is interacting with FtsZ1 proteins *in vivo*. However, due to their high sequence similarity and the limited number of matching peptides, the isoforms FtsZ1-1 and FtsZ1-2 could not be distinguished in these experiments. Hence, we were able to confirm that Physcomitrella FtsZ2-1 is interacting with Physcomitrella FtsZ1 proteins *in vivo*, but we could not explicitly narrow this down to an interaction with FtsZ1-2. Nevertheless, these findings suggest the formation of FtsZ1/FtsZ2 heteropolymers in Physcomitrella.

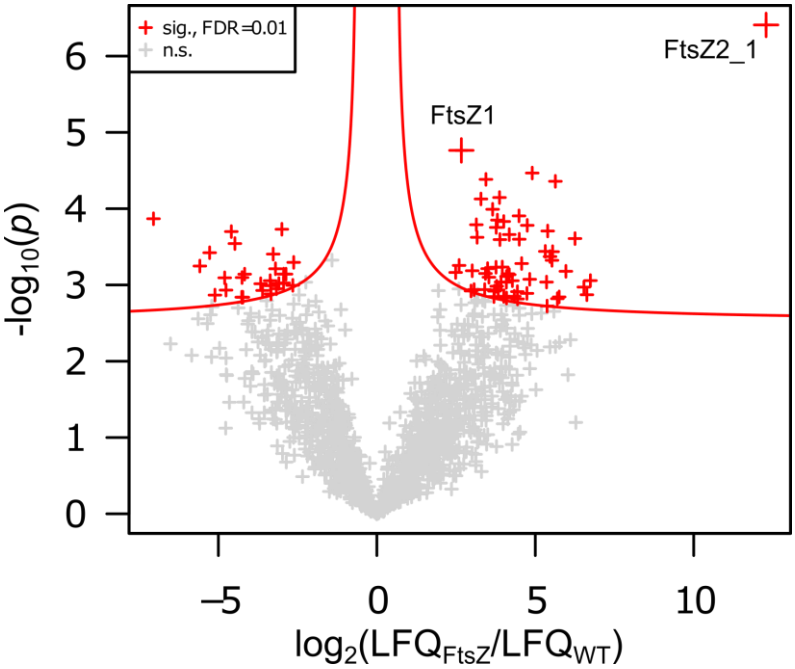

Figure 1: Analysis of the co-immunoprecipitations (Co-IPs) against GFP-tagged FtsZ2-1 protein. The Volcano plot shows the $\log_2$ ratios of normalized LFQ (label-free quantitation) intensities plotted against log10 of adjusted p-values. Proteins significantly enriched in the GFP-tagged pulldown are shown as red crosses with a false discovery rate (FDR) of 0.01 %. Physcomitrella wild type (WT) served as a negative control. Proteins not significant for neither WT nor FtsZ2-1-GFP are visualized as grey crosses. The Co-IP was performed with GFP-Trap Magnetic Particles M-270 (ChromoTek GmbH, Planegg, Germany) and Physcomitrella protonema tissue homogenized from suspension culture. The isoforms of FtsZ1 (FtsZ1-1, FtsZ1-2) could not be distinguished on the basis of the peptides identified in this approach and thus are grouped (FtsZ1).

3.2. Expression of Physcomitrella FtsZ1-2 and FtsZ2-1 in *E. coli*

The respective plastoskeletal morphologies of Physcomitrella FtsZ1-2 and FtsZ2-1, which were elucidated before (Özdemir et al., 2018), hint towards functional differences of these two isoforms. Therefore, the GTPase activity, polymer assembly, and formation of Physcomitrella FtsZ1-2 and FtsZ2-1 filaments *in vitro* were studied.

In order to produce Physcomitrella FtsZ1-2 and FtsZ2-1 in *E. coli*, the coding sequences (CDS) of both FtsZ isoforms were optimized for the codon usage in bacteria (Supplemental Figures S2 and S3). In total, 304 bases were changed for FtsZ1-2 and 357 bases were changed for FtsZ2-1. The GC content was concurrently increased from 49 % to 51 % for FtsZ1-2, and from 49 % to 52 % for FtsZ2-1. The *in-silico* predicted N-terminal transit peptides for Physcomitrella FtsZ1-2 (Pp3c19_2490) and Physcomitrella FtsZ2-1 (Pp3c11_17860) were 34 aa and 31 aa (ChloroP 1.1, http://www.cbs.dtu.dk/services/ChloroP/), respectively. The predictions of TargetP-2.0 (http://www.cbs.dtu.dk/services/TargetP/) and ChloroP 1.1 differ (Table 1) and the exact estimation of

cTPs remains challenging. The shorter predictions by ChloroP 1.1 were chosen so as not to affect the functional domains of both proteins.

Table 1 Comparison of sequence and length of the chloroplast transit peptide (cTP) for Physcomitrella FtsZ1-2 and FtsZ2-1 predicted by ChloroP 1.1 and TargetP-2.0. Length of cTP in amino acids (aa).

	Tool	predicted cTP sequence	length [aa]
FtsZ1-2	ChloroP 1.1	MGSTARLRLSPSPSSVSGSLCPASARSVYPMGSV	34
	TargetP-2.0	MGSTARLRLSPSPSSVSGSLCPASARSVYPMGSVAVRVTSRCRW LGAESRLGKSQFFGAGKPLVHLQKRGWSLGWEGRAAGRTVVM	86
FtsZ2-1	ChloroP 1.1	MALFSGCSGWAGLKVSSRVGGEACRTPPVVH	31
	TargetP-2.0	MALFSGCSGWAGLKVSSRVGGEACRTPPVVHCSMHSRSSVRA	42

The respective codon-optimized FtsZ1-2 and FtsZ2-1 sequence, fused to either a N- or C-terminal 8 x His-tag encoding sequence, were subcloned into the pLATE11 expression vector (Supplemental Tables S3 and S4) and with the correct plasmids subsequently transformed into BL21 Star™ (DE3) cells. For each of the differently tagged FtsZ constructs four resulting colonies were chosen for further analysis. These colonies were inoculated and protein production was induced by the addition of IPTG, simultaneously a non-induced culture of each clone was also investigated. After protein extraction the isoform production was analysed by SDS-PAGE followed by an anti-His immunoblot detection. In parallel, BL21 Star™ (DE3) containing the IPTG-inducible pLATE31-Cm plasmid encoding a His-tagged chloramphenicol acetyl transferase (CAT) was treated equivalently and served as a positive control.

While missing immunoblot signals for all non-IPTG induced samples proved that the expression of both isoforms depends on the induction by IPTG (Figure 2), only strains expressing the FtsZ1-2 and FtsZ2-1 variant with a C-terminal His-tag led to a detectable isoform production upon induction (Figure 2). The immunoblot signals matched the expected protein sizes for recombinant Physcomitrella (FtsZ1-2 44 kDa, FtsZ2-1 45 kDa). Based on these observations, one high producing clone of each C-terminal His-tagged Physcomitrella FtsZ variant was chosen for further experiments. The immunoblots and the Coomassie-stained SDS-gels for the FtsZ1-2 and FtsZ2-1 variant with a N-terminal His-tag are shown in Supplemental Figure S4.

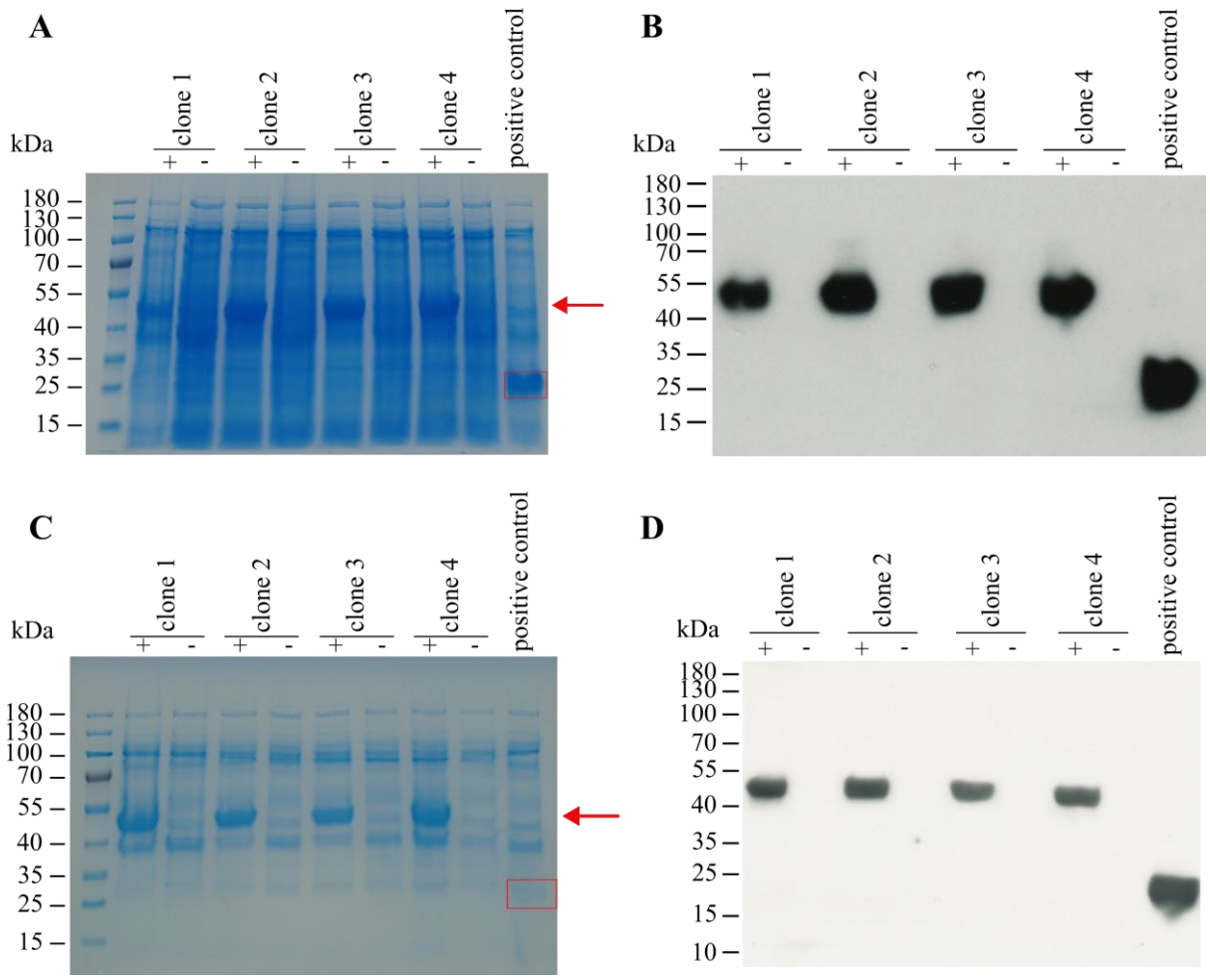

Figure 2 Coomassie-stained SDS gels and Immunoblot detection of BL21 Star™ (DE3) cells transformed with the pLATE11 expression vector for expression of Physcomitrella FtsZ1-2 and Physcomitrella FtsZ2-1 with C-terminal His-tags.
Total cell extracts of BL21 Star™ (DE3) cells transformed with the constructs for Physcomitrella FtsZ1-2 (A, B) and Physcomitrella FtsZ2-1 (C, D) were analysed by Coomassie-stained SDS-gels (A, C) and anti-His immunoblots (B, D). '+' and '-' signs indicate that the cells where either induced or not induced with IPTG. Red arrows indicate the overexpressed FtsZ1-2 and FtsZ2-1 proteins. The overexpression of His-tagged chloramphenicol acetyl transferase (red boxes) was used as a positive control.

3.3. Physcomitrella FtsZ proteins localize in foci in elongated *E. coli* cells

To investigate the behaviour of each isoform individually and in combination within a heterologous system, fluorescent FtsZ fusions were employed. *E. coli* FtsZ, which is non-functional in Physcomitrella and does not interact with Physcomitrella FtsZ isoforms in FRET experiments (Gremillon et al., 2007), is not anticipated to interact with Physcomitrella proteins. FtsZ1-2 was fused at the N-terminus with enhanced Green Fluorescent Protein (eGFP), while FtsZ2-1 was fused at the N-terminus with mKusabira-Orange2 (mKOrange2, mKO2). To serve as controls, eGFP-His and mKO2-His were used respectively. All CDS were cloned into the inducible pLATE11 expression vector. For the co-expression of eGFP-FtsZ1-2 and mKO2-FtsZ2-1, the latter expression cassette was introduced into the

initially generated pLATE11_eGFP-FtsZ1-2 vector. BL21 Star™ (DE3) cells were transformed with the final plasmids. Confocal microscopy of IPTG-induced bacteria revealed that the eGFP-His control was localized in a diffuse pattern within the cell (Figure 3A). The cells expressing eGFP-His grew normally and were approximately 1-2 µm long. The eGFP-FtsZ1-2 protein was localized in numerous foci within the cell (Figure 3B), and these foci appeared to be connected by thin filaments (Supplemental Figure S5). Cells expressing eGFP-FtsZ1-2 were longer than those expressing eGFP-His, showing a length distribution between 5 and 10 µm (Figure 3B, and Supplemental Figure S5A-E). The distribution of the eGFP-FtsZ1-2 signal suggests the assembly of functional structures, which is further supported by the filamentous phenotype of the *E coli* cells expressing eGFP-FtsZ1-2.

As with eGFP-His, the mKO2-His control exhibited a diffuse localization throughout the cell (Figure 3C). Cells transformed with mKO2-His also grew normally and were approximately 1-2 µm long. The mKO2-FtsZ2-1 protein was distributed in foci throughout the whole cell. The cells were elongated, ranging from 5 and 10 µm in length (Figure 3D, Supplemental Figure S6A-E). In analogy to eGFP-FtsZ1-2, we infer that eGFP-FtsZ2-1 also assembles in functional structures in transformed *E. coli* cells.

In general, the signal of mKO2-FtsZ2-1 in *E. coli* was weaker than the signal of eGFP-FtsZ1-2. Furthermore, it was observed that the foci of the mKO2-FtsZ2-1 were less frequent than in eGFP-FtsZ1-2 and were situated at regular intervals inside the cell. In contrast to eGFP-FtsZ1-2, no filaments between the foci of mKO2-FtsZ2-1 were observed.

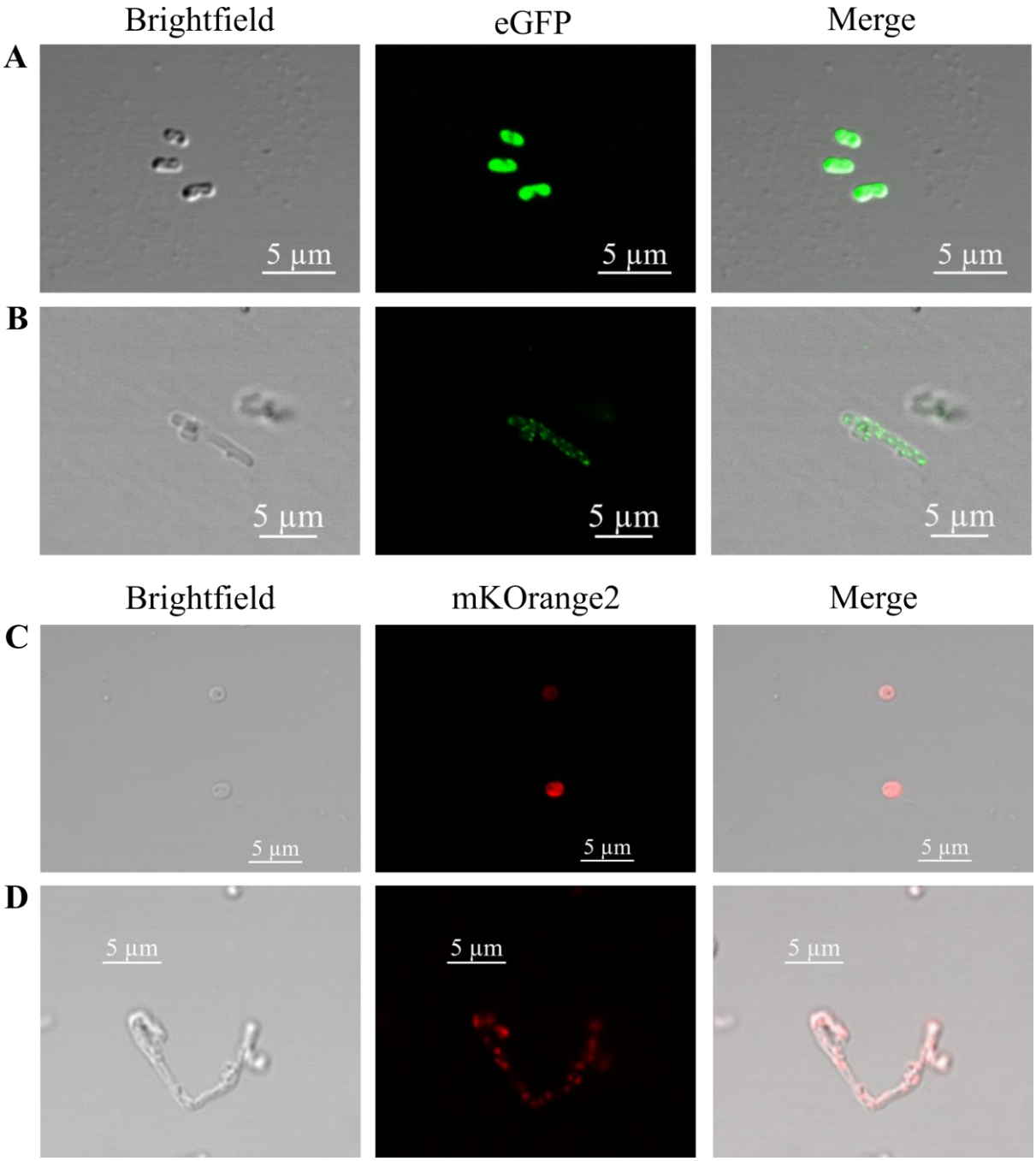

Figure 3 Cellular positioning of Physcomitrella FtsZ1-2 and FtsZ2-1 fluorescent fusion proteins in transformed *E. coli* cells.
Fluorescent microscopy of (A) eGFP-His, (B) eGFP-tagged Physcomitrella FtsZ1-2, (C) mKOrange2-His and (D) mKOrange2-tagged Physcomitrella FtsZ2-1 in *E. coli*. Scale bars as indicated.

Confocal microscopy of *E. coli* cells containing the double construct eGFP-FtsZ1-2_mKO2-FtsZ2-1 confirmed the heterologous expression of eGFP-FtsZ1-2 and mKO2-FtsZ2-1 in *E. coli* (Figure 4). Cells expressing eGFP-FtsZ1-2_mKO2-FtsZ2-1 were elongated and ranged between 5 and 20 µm in length (Figure 4, Supplemental Figure S7). In these cells, eGFP-FtsZ1-2 seemed once again localized in interconnected foci. Correspondingly, the distribution pattern of mKO2-FtsZ2-1 was similar as observed in the cells transformed with the single constructs: mKO2-FtsZ2-1 was distributed in foci

throughout the whole cell. Remarkably, it was observed that eGFP-FtsZ1-2 and mKO2-FtsZ2-1 co-localize in these foci within the cell (Figure 4) suggesting a direct or indirect interaction between the two proteins. Furthermore, it was observed that bacterial cells expressing eGFP-FtsZ1-2, mKO2-FtsZ2-1 and the construct with both FtsZ fusion proteins together exhibited highly aberrant phenotypes (Figure 3, Figure 4, Supplemental Figures S5, S6 and S7), suggesting that expression of the two moss FtsZ proteins affected bacterial cell division and shaping.

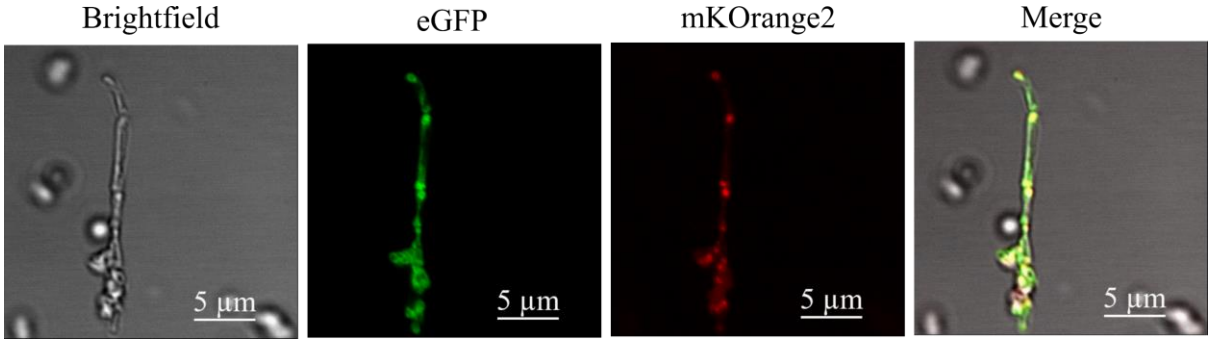

Figure 4 Cellular positioning of combined expression of Physcomitrella FtsZ1-2 and FtsZ2-1 fluorescent fusion proteins in *E. coli.*
Fluorescent microscopy of *E. coli* cells co-expressing eGFP-tagged Physcomitrella FtsZ1-2 and mKOrange2-tagged Physcomitrella FtsZ2-1. Scale bars as indicated.

3.4. Optimized purification of recombinant Physcomitrella FtsZ proteins

To study whether Physcomitrella FtsZ1-2 and FtsZ2-1 can potentially form plastoskeleton-like structures in the absence of other proteins, we set out to purify both proteins recombinantly produced in *E. coli*.

Overexpression and attempts of purification of the C-terminally his-tagged Physcomitrella FtsZ1-2 and FtsZ2-1 from *E. coli* revealed that both FtsZ proteins were partially localized in inclusion bodies. Purification of the FtsZ proteins not found in inclusion bodies using standard affinity purification protocols resulted in relatively low and highly contaminated protein amounts (Supplemental Figure S8). Attempts to further purify these proteins by for example size exclusion chromatography, were unsuccessful. Consequently, alternative approaches were explored. Initially, FtsZ1-2 was purified from the inclusion bodies under denaturing conditions in 6 M guanidine HCl, and refolding experiments were performed in different buffers. Although small amounts of refolded soluble proteins were obtained, the quantities of refolded FtsZ1-2 remained insufficient for subsequent gel filtration experiments and polymerization assays. Therefore, we set out to further optimize the expression strategies of both FtsZ isoforms. To enhance the stability of the FtsZ proteins and prevent formation of the inclusion bodies, Physcomitrella FtsZ1-2 and FtsZ2-1, lacking the N-terminal transit peptides of 86 and 42 amino acids, respectively (Table 1) were fused to an N-terminal His_6_SUMO-tag. Various expression conditions

were tested, and the highest amount of soluble protein was obtained after growth in a simplified version of autoinduction media at 25 °C (following Studier, 2014). Subsequently, the buffer composition used during the purification process was further optimized. Both proteins were more stable at higher pH of pH 10.6 and pH 9.5, respectively, and in the presence of 1 mM $MgCl_2$ and 5 % glycerol. FtsZ1-2 was more stable at 50 mM NaCl, whereas FtsZ2-1 was more stable at 250 mM NaCl. Therefore, the purification of FtsZ1-2 and FtsZ2-1 were performed in 25 mM glycine pH 10.6, 50 mM NaCl, 1 mM $MgCl_2$, 5 % glycerol and 50 mM glycine pH 9.5, 250 mM NaCl, 1 mM $MgCl_2$, 5 % glycerol, respectively. Using these optimized expression and purification conditions, high amounts of both proteins could be purified using Ni-affinity chromatography (Figures 5A and 6A). To remove the His_6_SUMO-tag, the pH was temporarily changed to 8.5 and pH 9.5, respectively, and the proteins were incubated with the SUMO-protease. During this step, the proteins also started to precipitate, but this could be reduced by the addition of 5 % glycerol. Following the removal of the His_6_SUMO-tag (Figures 5B and 6B), the pH was changed to 10 for FtsZ1-2, and kept at 9.5 for FtsZ2-1, and the proteins were further purified by size exclusion chromatography. This resulted in fractions containing highly pure FtsZ1-2 or FtsZ2-1, respectively (Figures 5C and 6C). Notably, FtsZ1-2 eluted significantly earlier from the size exclusion column then FtsZ2-1, a finding confirmed by analytical gel filtration experiments (Figures 5D and 6D). FtsZ1-2 (37.4 kDa) eluted corresponding to a mass of around 110 kDa (Figure 5D), suggesting purification in an oligomeric form, possibly a trimer. In contrast, FtsZ2-1 (43.4 kDa) eluted corresponding to a mass of 44 kDa (Figure 6D), indicating purification as a monomer. Unfortunately, attempts to increase protein concentrations beyond approximately 25 µM or removing glycerol from the buffer resulted in precipitation of both FtsZ proteins, limiting the concentrations and conditions suitable for further experiments.

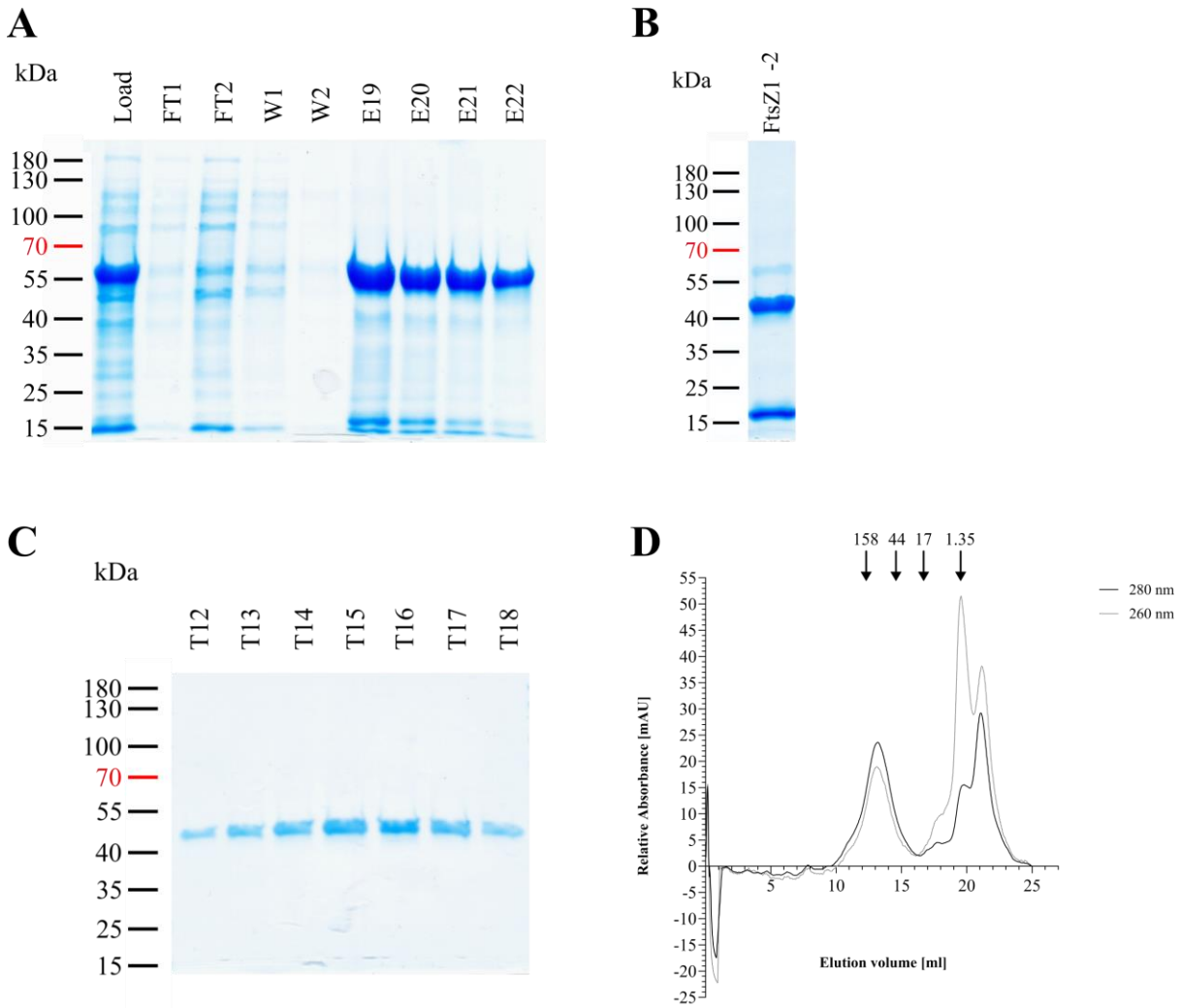

Figure 5 Purification of FtsZ1-2.
Coomassie blue-stained SDS-PAGE analysis of the purification steps for FtsZ1-2. (A) Fractions obtained during Ni-affinity chromatography, including flow-through (FT), wash (W), and elution (E) samples, labelled with tube numbers. (B) Coomassie blue-stained SDS-PAGE of FtsZ1-2 after SUMO-protease digestion. (C) Coomassie blue-stained SDS-PAGE of FtsZ1-2-containing fractions after gel filtration on a Superdex 200 16/600 size exclusion column. (D) Gel filtration elution profiles of FtsZ1-2 on a Superdex 200 10/300 size exclusion column, with absorption measured at 260 nm and 280 nm. Arrows indicate the elution maxima of marker proteins (gamma-globulin 158 kDa, ovalbumin 44 kDa, myoglobin 17.1 kDa, and vitamin B12 1.35 kDa). The expected molecular masses of His_6_SUMO_FtsZ1-2 and FtsZ1-2 are 49.7 kDa and 37.4 kDa, respectively.

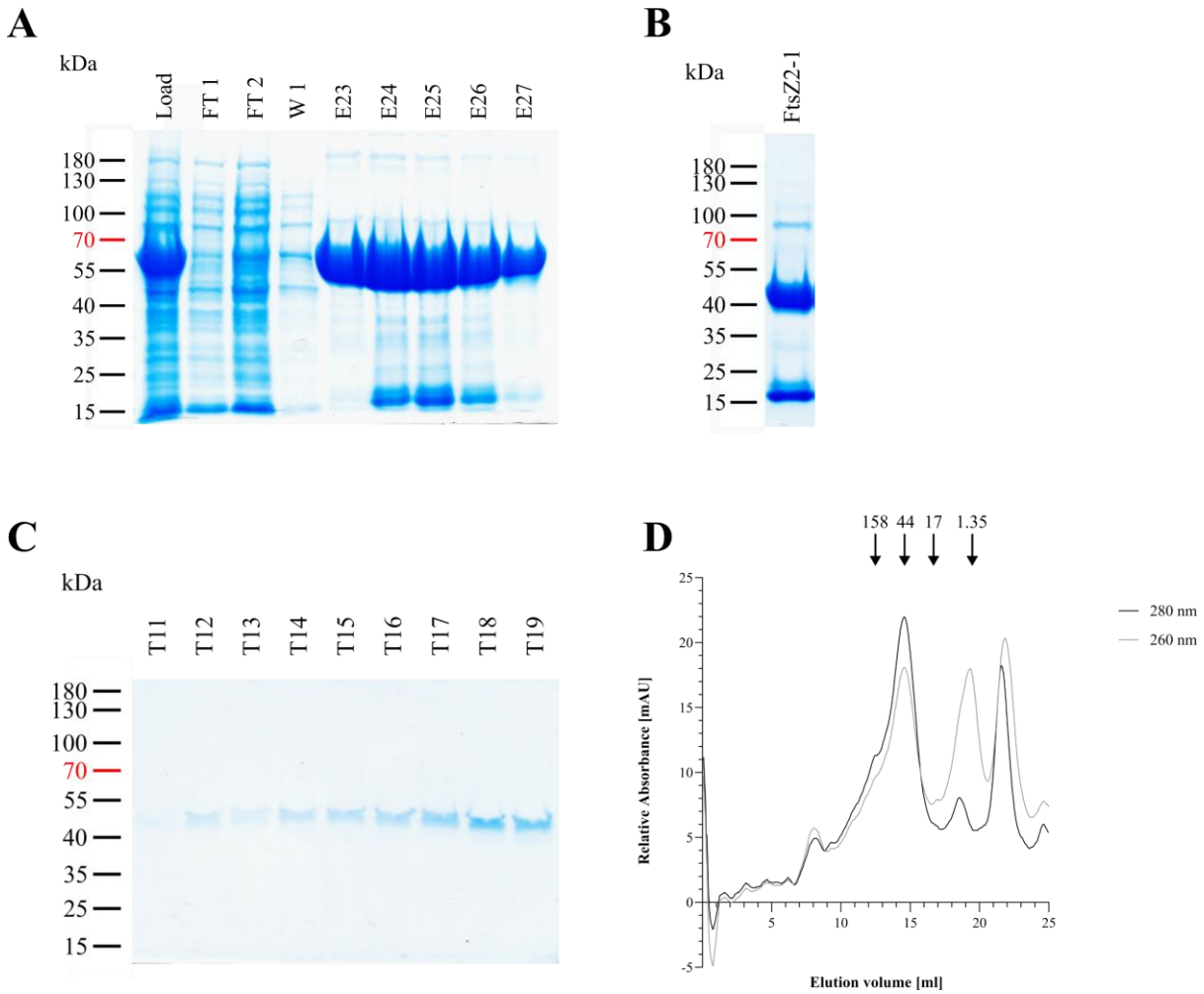

Figure 6 Purification of FtsZ2-1.
Coomassie blue-stained SDS-PAGE analysis of the purification steps for FtsZ2-1. (A) Fractions obtained during Ni-affinity chromatography, including flow-through (FT), wash (W), and elution (E) samples, labelled with tube numbers. (B) Coomassie blue-stained SDS-PAGE of FtsZ2-1 after SUMO-Protease digestion. (C) Coomassie blue-stained SDS-PAGE of FtsZ2-1-containing fractions after gel filtration on a Superdex 200 16/600 size exclusion column. (D) Gel filtration elution profiles of FtsZ2-1 on a Superdex 200 10/300 size exclusion column, with absorption measured at 260 nm and 280 nm. Arrows indicate the elution maxima of marker proteins (gamma-globulin 158 kDa, ovalbumin 44 kDa, myoglobin 17.1 kDa, and vitamin B12 1.35 kDa). The expected molecular masses of His_6_SUMO_FtsZ2-1 and FtsZ2-1 are 55.8 kDa and 43.3 kDa, respectively.

3.5. Physcomitrella FtsZ proteins show GTPase activity *in vitro*

After conducting analytical gel filtration experiments to confirm correct folding of FtsZ1-2 and FtsZ2-1, the GTPase activity of both isoforms was measured *in vitro* using the Malachite Green assay adapted from Król & Scheffers (2013). To identify a buffer suitable for the Physcomitrella FtsZ GTPase assays, we investigated the influence and significance of different buffer components. The GTPase activity of *E. coli* FtsZ is promoted by KCl, but not NaCl (Mukherjee et al., 1993). Therefore, the pH (6.5-8.5), [NaCl] (50-300 mM) and [KCl] (0-300 mM) were tested, but only very low GTPase activities were measured. Remarkably, the GTPase activity increased significantly when NaCl in the buffer was

replaced by KCl, suggesting that NaCl might inhibit Physcomitrella FtsZ activity. After a buffer exchange replacing NaCl with KCl, the GTPase activity of both isoforms was measured separately and together as a function of protein concentration (Figure 7). Both FtsZ proteins showed low but significant GTPase activities, with FtsZ1-2 displaying higher activity than FtsZ2-1. Stoichiometric mixing of both FtsZ isoforms did not result in an increase of the overall measured GTPase activity, indicating that there is no stimulating or inhibiting interaction between the two FtsZ isoforms.

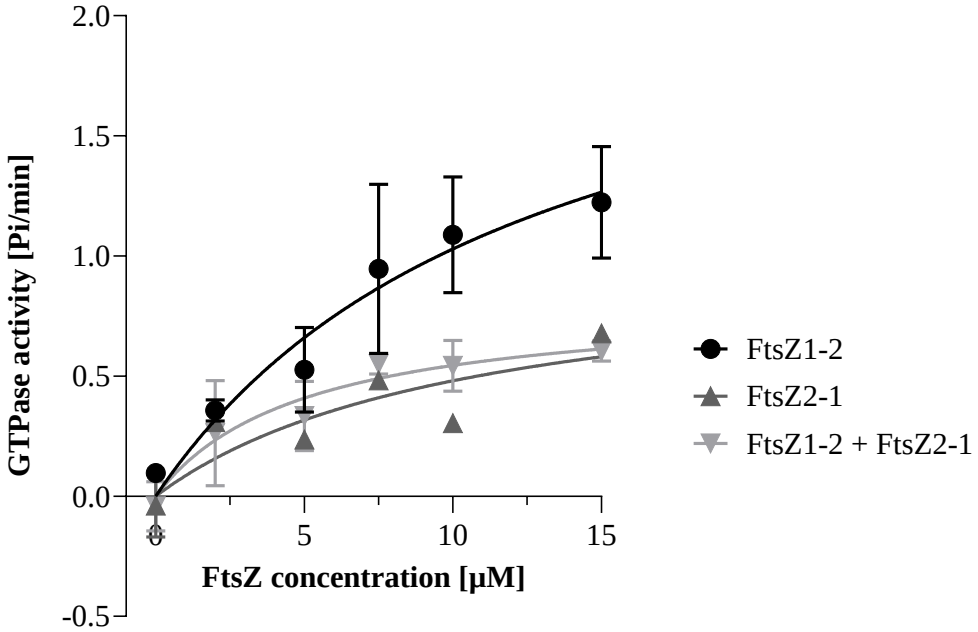

Figure 7 GTPase activity of Physcomitrella FtsZ1-2 and FtsZ2-1.
GTPase assays were performed at 25 °C with FtsZ1-2 and FtsZ2-1 separately, and FtsZ1-2 and FtsZ2-1 together. The assay was modified after Król & Scheffers (2013) and performed with malachite green. Assays were performed with increasing FtsZ concentrations in the presence of 1 mM GTP. The amount of free phosphate [µM] per minute was calculated based on the phosphate standard calibration curve at 600 nm. n = 2, replicates with standard deviation.

3.6. *In vitro*-polymerization of Physcomitrella FtsZ1-2

In *E. coli*, GTP hydrolysis by FtsZ is closely associated with the formation of FtsZ filaments (Mukherjee, 1998). Following the GTPase assays and confirming the GTPase activity of both Physcomitrella FtsZ isoforms *in vitro*, the *in-vitro* formation of filaments was studied using light scattering assays. Light scattering assays are a valuable method for visualizing FtsZ filament formation in real-time, as light scattering is proportional to the mass of polymers formed (Mukherjee and Lutkenhaus, 1999). The light scattering experiments were performed under the same conditions as the GTPase assays (Figure 8).

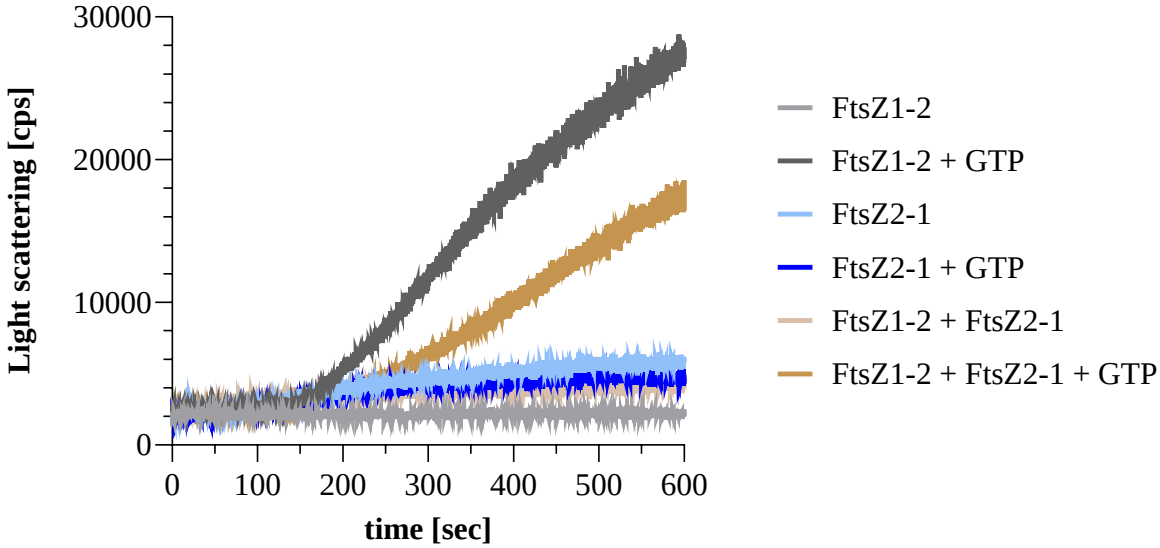

Figure 8 Light scattering experiments with FtsZ1-2, FtsZ2-1 individually, and FtsZ1-2 and FtsZ2-1 together.
Light scattering experiments were performed at 25 °C, both in the presence or absence of GTP. GTP was added after 50 sec at a final concentration of 1 mM. The reaction was monitored for 600 sec. Light scattering in counts per seconds (cps). Experiments were carried out with 15 µM FtsZ1-2, 15 µM FtsZ2-1 or 7.5 µM FtsZ1-2 and 7.5 µM FtsZ2-1.

Upon addition of GTP, an increase in light scattering was observed in the presence of 15 µM FtsZ1-2, suggesting that this isoform is capable of forming filaments in the presence of GTP. The increase was notable but relatively slow when compared to other plant FtsZ proteins at similar concentrations (Porter et al., 2021; Porter et al., 2023). Remarkably, no increase in light scattering could be observed when the experiment was performed with buffer containing NaCl, once again suggesting that NaCl inhibits polymerization of FtsZ1-2. Conversely, no increase in light scattering could be observed for 15 µM FtsZ2-1. When light scattering experiments were performed with 7.5 µM FtsZ1-2 and 7.5 µM FtsZ2-1, a light scattering signal with the intensity expected for 7.5 µM FtsZ1-2 was observed. Thus, within these experiments, increased light scattering was observed for FtsZ1-2 upon addition of GTP, but no indication of an interaction between FtsZ1-2 and FtsZ2-1 could be found.

3.7. GTP-dependent filament formation of FtsZ1-2 and FtsZ2-1

Both FtsZ1-2 and FtsZ2-1 exhibited low GTPase activity *in vitro*. FtsZ1-2, but not FtsZ2-1, showed an increase in light scattering upon the addition of GTP, indicative of filament formation. The possible formation of FtsZ filaments was independently studied by negative stain transmission electron microscopy. Under the same conditions as used for the GTPase and the light scattering experiments, some filaments could be observed for both FtsZ1-2 and FtsZ2-1 when they were incubated in the presence of 2 mM GTP (Figure 9), while no filaments were observed in the absence of GTP (Supplemental Figure S9). This demonstrates that both FtsZ isoforms are capable of forming filaments

in a GTP-dependent manner. When FtsZ1-2 and FtsZ2-1 were co-incubated in the presence of GTP, similar filaments were observed. However, it was not possible to distinguish between FtsZ1-2, FtsZ2-1 or possible FtsZ1-2/FtsZ2-1 filaments (Figure 9).

In conclusion, purified Physcomitrella FtsZ1-2 and FtsZ2-1 are active and both can form filaments. Remarkably, no interaction between these isoforms was observed *in vitro*, while the *in-vivo* data in Physcomitrella and in *E. coli* suggest such an interaction.

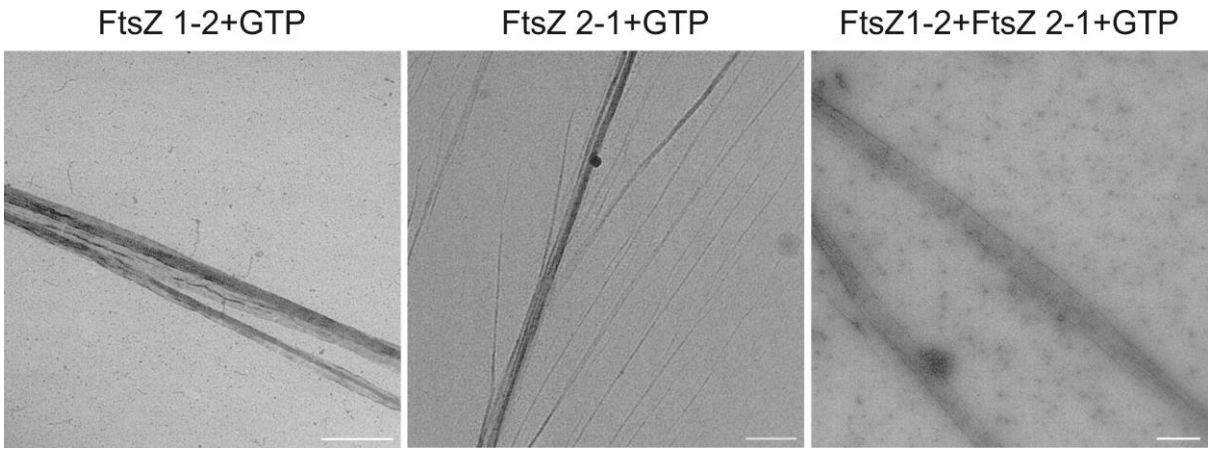

Figure 9 Negative stain transmission electron microscopy of Physcomitrella FtsZ filaments. 15 µM of FtsZ1-2 (left), 15 µM FtsZ2-1 (middle) and 7.5 µM FtsZ1-2 mixed with 7.5 µM FtsZ2-1 (right) were incubated at room temperature for 5 min with 2 mM GTP and then imaged by transmission electron microscopy. Representative images are shown. Scale bar is 1 µm. Experiments were repeated with two independent purifications with similar results.

4. Discussion

FtsZ proteins are GTPases and GTP hydrolysis is a prerequisite for their polymerization (de Boer et al., 1992; Smith et al., 2010; Porter et al., 2021). The moss Physcomitrella encodes the high number of five different FtsZ proteins, suggesting neofunctionalisation of the different isoforms during evolution (Rensing et al., 2004; Martin et al., 2009a; Grosche & Rensing, 2017). The interplay among the five FtsZ isoforms results in the formation of a filament network inside the chloroplasts, where each isoform exhibits distinct filament characteristics (Özdemir et al., 2018). Two of the five isoforms (FtsZ1-2, FtsZ2-1) have relatively high expression levels in various moss tissues, indicating division-independent, stable networks within the chloroplast (Özdemir et al., 2018). Knowledge about the polymer-forming properties of FtsZ1-2 and FtsZ2-1 as a GTP-driven non-equilibrium structure is of particular interest to develop sustainable material systems (Özdemir et al., 2019). Here, we expressed FtsZ1-2 and FtsZ2-1 in *E. coli*. We monitored the localization of fluorescence-tagged Physcomitrella FtsZ in *E. coli* cells after induction, established a purification protocol the recombinant FtsZ isoforms, and characterized their GTPase activity and polymerization mechanism *in vitro*.

Expression of fluorescence-tagged Physcomitrella FtsZ1-2 and FtsZ2-1 in *E. coli* resulted in fluorescent foci and elongated cells. The distribution pattern of fluorescence-tagged Physcomitrella FtsZ is similar to *E. coli* FtsZ tagged with GFP (Ma et al., 1996). Higher levels of *E. coli* FtsZ tagged with GFP also localized in foci and the over-expression of *E. coli* FtsZ of at least 10-fold above WT levels also inhibits cell division, resulting in filamentous cell shapes (Ward and Lutkenhaus, 1985; Ma et al., 1996). The foci at higher FtsZ concentration could represent FtsZ nucleation sites, as suggested by Ma et al. (1996). In contrast, *Synechococcus elongatus* FtsZ tagged with mCerulean and Arabidopsis FtsZ1 tagged with mVenus localize to long curved filaments when expressed separately in yeast (Porter et al., 2023). The localization of Physcomitrella FtsZ1-2 and FtsZ2-1 in *E. coli* indicates that the FtsZ function is evolutionary conserved and that Physcomitrella FtsZ interferes with cell division and morphology when overexpressed in *E. coli*.

To analyse the *in vitro*-polymerization of both Physcomitrella FtsZ isoforms individually and in combination, GTPase assays and light scattering assays were performed with the recombinant proteins. Both assays were performed with up to 15 µM of Physcomitrella FtsZ1-2 and FtsZ2-1. During the assay time of 10 min, only FtsZ1-2, but not FtsZ2-1, slowly polymerized in the presence of GTP. Nevertheless, both isoforms show GTP-dependent polymerisation in TEM. Different protocols for GTPase assays as well as *in vitro*-polymerization assays of bacterial FtsZ have been established. They differ mainly in the concentrations of purified FtsZ in the assays, ranging from 8 µM *Agrobacterium tumefaciens* FtsZ (Howell et al., 2019) to 12 µM *Bacillus subtilis* FtsZ and 12 µM of *E. coli* FtsZ (Król & Scheffers, 2013). Notably, *E. coli* FtsZ polymerizes very rapidly and reaches a steady-state within only 30 seconds (Mukherjee and Lutkenhaus, 1999). In GTPase assays with renatured Arabidopsis FtsZ1 and FtsZ2 5 µM purified protein was used (Olson et al., 2010), while GTP assays with soluble Arabidopsis FtsZ were performed with 0.2 to 3 µM for AtFtsZ1 and 0.5 to 6 µM for AtFtsZ2. For light scattering assays, up to 7 µM Arabidopsis FtsZ2 was used, and after around 10 min FtsZ2 assembled to polymers and, depending on the concentration, reached its plateau or started depolymerizing (Porter et al., 2021). In contrast, even at the Physcomitrella FtsZ concentration of 15 µM, the GTPase activities were low and increase in light scattering was slower than most other characterized FtsZ proteins.

Our results support the idea (Porter et al., 2023) that a low GTPase activity of plant FtsZ proteins compared to bacterial FtsZ is a conserved feature. One reason might be that bacteria divide faster than chloroplasts, and thus require a higher GTPase activity and faster assembly of the Z-ring. In contrast to bacteria, chloroplasts are not able to divide on their own as chloroplast division relies on additional nuclear-encoded proteins (Okazaki et al., 2010). This implies that only the initiation of chloroplast division itself might take as much time as the whole division process in bacteria. Furthermore, plant-specific components of the division machinery are involved in the rate of chloroplast division, e.g. PLASTID DIVISION (PDV) proteins. The overexpression of PDV proteins in both Arabidopsis and Physcomitrella led to an increase in chloroplast number and a decrease in chloroplast size (Okazaki et al., 2009). Additionally, the rates of chloroplast division might vary depending on the developmental

stage: during leaf development the level of PDV proteins decreased, leading to a decrease in the chloroplast division rate (Okazaki et al., 2009). This indicates another mechanism determining the rate of chloroplast division, which might explain why chloroplasts take more time to divide, therefore not depending on a high FtsZ GTPase activity. Thus, the relatively slow GTP-dependent polymerization of the Physcomitrella FtsZ proteins at relatively high concentrations observed here is in accordance with their participation in a plastoskeleton, which persists independent of the division process. To corroborate this, we aim to perform similar experiments with the three other Physcomitrella FtsZ isoforms, which are known to have lower expression levels in various moss tissues.

In accordance with neofunctionalisation during evolution, Physcomitrella FtsZ1-2 and FtsZ2-1 have different GTPase-activity levels when investigated individually. Differences in the GTPase activity and polymerization mechanism of FtsZ homologues of the same organism were observed before. The gram-negative bacterium *Rhizobium radiobacter* (formally called *Agrobacterium tumefaciens*) contains three FtsZ isoforms (Zupan et al., 2013). For two of them ($FtsZ_{AT}$, $FtsZ_1$) the GTPase activity and the ability to form filaments was investigated independently. Only $FtsZ_{AT}$ hydrolyses GTP, polymerizes in light scattering experiments and forms protofilaments in the presence of GTP. In contrast, $FtsZ_1$ showed no GTPase activity, no polymer formation in TEM and no polymerization in light scattering, even at concentrations of 8 µM (Howell et al., 2019). Similarly, Arabidopsis FtsZ1 and FtsZ2 have different GTPase activities and polymerization mechanisms (Osteryoung et al., 1998; Porter et al., 2021), demonstrating that they have different assembly properties when assayed separately *in vitro* (Porter et al., 2021).

By performing Co-IPs, it was confirmed that Physcomitrella FtsZ2-1 interacts with Physcomitrella FtsZ1 proteins *in vivo*. In FRET experiments, the *in-vivo* interaction between Physcomitrella FtsZ2-1 and FtsZ1-1 was observed before (Gremillon et al., 2007). Our Co-IPs were performed with an in-frame fusion of Physcomitrella FtsZ2-1 with GFP at the endogenous locus and not with over-expression lines. Because of rather low abundance and high similarity of these isoforms, the interacting FtsZ1 isoform could not be unambiguously specified by the identified peptides. Consequently, it was decided not to follow up on the approach to estimate the ratio of FtsZ1-2 and FtsZ2-1 forming (hetero)polymers but to perform GTPase assays and polymerization assays with a mixture of Physcomitrella FtsZ1-2 and FtsZ2-1 in a 1:1 ratio. This mixing did not result in a change of the overall GTPase activity, suggesting that there is no stimulation or inhibition caused by the interaction of the two FtsZ isoforms. This result is consistent with findings regarding Arabidopsis FtsZ proteins (Porter et al., 2021). Nonetheless, we currently lack an explanation for this observation. Since no high GTPase activity of Physcomitrella was observed for FtsZ2-1 alone, it is likely that the activity measured when mixing both isoforms is due to the GTPase activity of FtsZ1-2 alone. Furthermore, this indicates that the *in-vivo* interaction of FtsZ1-2 and FtsZ2-1 is independent of their individual GTPase activity and polymerization mechanism or would require conditions different from our *in-vitro* set-up.

We were able to visualize protofilaments for both Physcomitrella FtsZ isoforms in negative stain TEM and saw differences in filament morphology. Filaments of FtsZ2-1 were more filigree than FtsZ1-2, which aligns with our observations with mKO2-tagged FtsZ2-1 in *E. coli*. Differences in the polymer-forming abilities of plant FtsZ proteins were observed before. Arabidopsis FtsZ2 has similar filaments as Physcomitrella FtsZ1-2 in TEM, while Arabidopsis FtsZ1 does not assemble in filaments on its own in TEM at the tested conditions (Porter et al., 2021). In Physcomitrella, FtsZ2-1 is directly involved in plastid division (Strepp et al., 1998; Khraiwesh et al., 2008) leading to enlarged plastids in basal chloronema cells of the Δ*ftsZ2-1* mutant (Martin et al., 2009b). Furthermore, chloroplasts of Δ*ftsZ2-1* cells show complete loss of chloroplast integrity (Özdemir et al., 2018). In contrast, chloroplasts in the chloronema cells of the Δ*ftsZ1-2* mutant did not show morphological differences compared to WT cells (Özdemir et al., 2018). This indicates that FtsZ2-1 is essential for maintaining chloroplast shape and integrity, while FtsZ1-2 might be less important. Moreover, the fact that we found differences in the GTPase activity and polymerization mechanism of Physcomitrella FtsZ1-2 and FtsZ2-1 is in accordance with the fact the respective plastoskeletal morphologies for these isoforms differ *in vivo*. While FtsZ2-1 filaments are exclusively formed within the chloroplast, FtsZ1-2 filaments apparently need to be longer, as they form long, extra-plastidic extensions to connect multiple chloroplasts *via* stromules (Suppanz et al., 2007; Özdemir et al., 2018). In general, it is reasonable to assume that differences in filament morphology are due to the underlying differences in GTPase activity and polymerization dynamics.

Taken together, we found GTPase activity and *in-vitro* polymerization of Physcomitrella FtsZ1-2 and low GTPase activity of Physcomitrella FsZ2-1. We confirmed the individual (homo)polymer formation of both FtsZ isoforms using TEM and showed that Physcomitrella FtsZ1 isoforms were identified as significant interactors of Physcomitrella FtsZ2-1 *in vivo*. We present the heterologous expression of eGFP-tagged Physcomitrella FtsZ1-2 and mKO2-tagged FtsZ2-1 in *E. coli*. The observation that the over-expression of Physcomitrella FtsZ1-2 and FtsZ2-1 in *E. coli* leads to elongated cells confirms that the FtsZ function for bacterial and organelle division is evolutionary conserved. Furthermore, our results provide insights into the polymer-forming properties of Physcomitrella FtsZ1-2 and FtsZ2-1. Based on the mutant phenotypes (Martin et al., 2009b, Özdemir et al., 2018) the localization of Physcomitrella FtsZ in *E. coli* (this study), the *in vivo* (Özdemir et al., 2018 and this study) and our *in-vitro* studies, we postulate different roles for FtsZ1-2 and FtsZ2-1 regarding the assembly of the plastoskeleton. Physcomitrella FtsZ2-1 might be more involved in chloroplast division and shaping, which, taken together with its lower GTPase activity, supports the idea (Porter et al., 2023) that the low GTPase activity of chloroplast FtsZ proteins compared to bacterial FtsZ is a conserved feature. FtsZ1-2 on the other hand might be more involved in chloroplast-chloroplast interaction *via* highly dynamic stromule formation, which needs longer filaments and a higher GTPase activity. These diverse functions of FtsZ1-2 and FtsZ2-1, as well as their interaction, impact the formation of the Physcomitrella plastoskeleton, abidingly shaping chloroplast morphology.

5. Materials and Methods

5.1. Design of the expression vectors FtsZ1-2 and FtsZ2-1

The coding sequences (CDS) for *Pp*FtsZ1-2 (Pp3c19_2490) and *Pp*FtsZ2-1 (Pp3c11_17860) according to the latest Physcomitrella genome version (Lang et al., 2018) were optimized for bacterial expression. Changes in the CDS were made accordingly to a codon usage table derived from the analysis of 16,000 *E. coli* genes using a custom Perl script (Wall et al., 2000) and the GC content was concurrently increased (script written by Dr. Oguz Top). The putative N-terminal transit peptides for *Pp*FtsZ1-2 (Pp3c19_2490) and *Pp*FtsZ2-1 (Pp3c11_17860) were determined using the ChloroP 1.1 Prediction Server (http://www.cbs.dtu.dk/services/ChloroP/). The codon-optimized sequences lacking the predicted N-terminal transit peptides (34 and 32 amino acids, respectively, Table 1) were synthesized by Eurofins Genomics Germany GmbH, Ebersberg, Germany. For cloning of the final construct of FtsZ2-1, the primers were designed starting at amino acid 33. The fragments for FtsZ1-2 and FtsZ2-1 were amplified via PCR using the respective primers (Supplemental Tables S3 and S4). The final expression vectors were subcloned into the pLATE11 bacterial expression vector via Ligation Independent Cloning (LIC, aLICator LIC Cloning and Expression Kit 1, untagged; Thermo Fisher Scientific, Waltham, USA) following the manufactures' instructions. The pLATE11 expression vector allows high levels of target protein expression. The 8 x His-tag was integrated into the primer and added either to the N- terminus or the C-terminus of the CDS.

5.2. Design of the expression vectors pLATE_eGFP_His, pLATE_eGFP_FtsZ1-2_His, pLATE_mKO2_His, pLATE_mKO2_FtsZ2-1_His

To generate the expression vectors pLATE_eGFP_His, pLATE_eGFP_FtsZ1-2_His, pLATE_mKO2_His, pLATE_mKO2_FtsZ2-1_His, the CDS of FtsZ1-2, FtsZ2-1, eGFP and mKOrange2 (mKO2) were amplified via PCR using the respective primers (Supplemental Table S3 and S4). The mKO2 template was kindly provided by Dr. Roland Nitschke. The inserts were then assembled via Gibson cloning (Gibson et al., 2009) and subcloned into the pJET1.2 vector (CloneJET PCR cloning kit, Thermo Fisher Scientific) following the manufactures' instructions. After identification of the recombinant clones, the correct construct was used as template to be amplified using the respective primers for LIC cloning (Supplemental Table S3). The PCR fragments were subcloned into the pLATE11 expression vector via Ligation Independent Cloning following the manufactures' instructions. To create the construct containing both fluorescence-tagged FtsZ isoforms, the pLATE_eGFP_FtsZ1-2_His vector was linearized using Nde I. Subsequently, the mKO2-FtsZ2-1 expression cassette, amplified from the pLATE_mKO2_FtsZ2-1_His vector, was inserted into the corresponding site by Gibson cloning.

Table 2 Plasmids used in this study

Plasmid	Relevant characteristics
pLATE_FtsZ1-2_His_8	Overproduction FtsZ1-2 with C-terminal His_8
pLATE_FtsZ2-1_His_8	Overproduction FtsZ2-1 with C-terminal His_8
pLATE_eGFP_His_8	Overproduction eGFP with His_8
pLATE_eGFP_FtsZ1-2_His_8	Overproduction FtsZ1-2 with N-terminal eGFP and C-terminal His_8
pLATE_mKOrange2_His_8	Overproduction mKOrange2 with His_8
pLATE_mKOrange2_FtsZ2-1_His_8	Overproduction FtsZ2-1 with N-terminal mKOrange2 and C-terminal His_8
pLATE_eGFP_FtsZ1-2_His_8_ mKOrange2_FtsZ2-1_His_8	Overproduction FtsZ1-2 with N-terminal eGFP and C-terminal His_8 and overproduction FtsZ2-1 with N-terminal mKOrange2 and C-terminal His_8
His_6_SUMO_FtsZ1-2	Overproduction FtsZ1-2 with N-terminal His_6 and SUMO-tag
His_6_SUMO_FtsZ2-1	Overproduction FtsZ2-1 with N-terminal His_6 and SUMO-tag
pLATE31-Cm	Overproduction CAT

5.3. Design of the expression vectors His_6_SUMO_FtsZ1-2 and His_6_SUMO_FtsZ2-1

The CDS of FtsZ1-2 and FtsZ2-1 lacking the N-terminal transit peptides (86 and 42 amino acids, respectively) were amplified via PCR (Supplemental Table S4) and subcloned into the linearized pSVA13429 vector (Nußbaum et al., 2023) via Gibson cloning (Gibson et al., 2009). The final vectors were sequenced with SUMO_fwd and T7_rev (Supplemental Table S4).

5.4. Transformation of E. coli BL21 Star™ (DE3) cells

BL21 Star™ (DE3) One Shot® (Invitrogen, Thermo Fisher Scientific) cells were transformed with the different vectors listed in Table 2 according to the manufacturer's instructions.

5.5. Generation of a FtsZ2-1-eGFP fusion line

The coding sequence of eGFP combined with a flexible 18 bp linker (Tian et al., 2004) fused FtsZ2-1 at the endogenous locus via homologous recombination as described (Hoernstein et al., 2023). Homologous flanks for the integration were chosen to remove the endogenous stop codon. Restriction site for Esp3I to release the linearized transfection construct from the final vector backbone were included at the 5' and the 3' end of the knock-in construct. All necessary parts were amplified with Phusion polymerase (Thermo Scientific) and assembled into the pJet1.2 vector backbone (Thermo Fisher Scientific) via triple template PCR as described (Tian et al., 2004). PCR's were performed with

the primers listed in Supplemental Table S1. The plasmid linearized *via* Alw26I digestion as well as a plasmid for co-transfection containing a neomycin resistance cassette (Mueller et al., 2014) were purified via ethanol precipitation (Sambrook and Russell, 2006) and transfection and selection was performed as described (Hohe and Reski, 2002; Hohe et al., 2004). Plants surviving the selection procedure were screened by PCR (Phire Polymerase, Thermo Scientific) for targeted integration of the knock-in construct at the desired locus as described (Hoernstein et al., 2023). Sequences of primers used for cloning and screening are listed in Supplemental Table S3. Physcomitrella WT as well as the employed eGFP fusion line #516 is available from the International Moss Stock Centre (IMSC, www.moss-stock-center.org) with accessions 40001 and 40960, respectively. The plasmid containing the knock-in construct is also available from the IMSC under accession P1779.

5.6. Co-immunoprecipitation

Co-immunoprecipitations of the GFP-tagged FtsZ2-1 line was performed in biological triplicates using GFP-Trap Magnetic Particles M-270 (Chromotek, Planegg-Martinsried, Germany). In brief, 300 mg homogenized protonema of the bait line (GFP-tagged FtsZ2-1, line #513) and WT were dissolved in 2 mL ice-cold extraction buffer (25 mM HEPES-KOH, pH 7.5, 2 mM EDTA, 100 mM NaCl, 200 nM DTT, 0.5 % Triton X-100, 1 % plant protease inhibitor cocktail (PPI, P9599, Sigma Aldrich, St. Louis, USA). All further steps were performed as described (Hoernstein et al., 2023). MS analyses were performed on a Q-Exactive Plus instrument (Thermo Fisher Scientific) coupled to an UltiMate 3000 RSLCnano system (DionexRef to Philipps PRC paper (should come out in nat micro hopefully this week. Otherwise refer to the paper on bioarchivesPackings/Thermo Fisher Scientific) as described (Top et al., 2021). Database search of the test Co-IP's was performed with Mascot Server V2.7.0 (Matrix Science). Results were subsequently loaded in Scaffold™ 5 software (V5.0.1, Proteome Software) and proteins were accepted at an FDR = 1 and peptides at an FDR = 0.5. Database search and label free quantitation of the quantitative CoIP were performed as described in Hoernstein et al. (2023) using *MaxQuant* (2.1.4.0; Cox and Mann, 2008). The database contained all Physcomitrella V3.3 protein models (Lang et al., 2018) as well as a fusion sequence of FtsZ2.1 (Pp3c11_17860) and eGFP Data analysis was performed in Perseus (V2.0.10.0, (Tyanova et al., 2016). Proteins with at least two LFQ values in at least one group (FtsZ or WT) were used and missing values were imputed from a normal distribution with a down-shift of 1.8 and distribution width of 0.5. True interaction partners were accepted at an FDR of 0.01 % and a p-value < 0.01. The resulting table containing significantly interacting proteins is available from Supplemental Table S2.

5.7. Preparation of transformed BL21 Star™ (DE3) cells for confocal microscopy

For confocal microscopy, 3ml of LB medium containing 50 mg/ml ampicillin (amp) and 1 % glucose was inoculated with a colony of respective transformed BL21 Star™ (DE3) cells, picked from a LB/amp

agarose plate. The inoculated culture was then incubated overnight at 37°C while shaking. On the subsequent day, 200 µL of this overnight culture was transferred to 2.8 mL of LB/amp and further incubated for 3 hours at 37°C. Subsequently, 0.5 mM isopropyl ß D thiogalactopyranoside (IPTG) was added, and the culture was incubated for an additional 45 minutes. For confocal microscopy, 1-5 µL of the respective bacterial solution was transferred to a microscopy glass slide. Then the samples were embedded using ProLong™ Glass Antifade Mountant (Thermo Fisher Scientific), covered with a cover slide, and stored in darkness for 24 hours prior to confocal microscopy.

5.8. Confocal microscopy of transformed BL21 Star™ (DE3) cells

All images were taken with a Zeiss LSM880 NLO microscope (Carl Zeiss Microscopy GmbH, Jena, Germany) using Plan-Apochromat 40x/1.4 Oil DIC(UV)VIS-IR objective with a zoom factor of 2. For the excitation the laser was applied at 488 nm (eGFP) or 561 nm (mKO2) with an intensity of 2 % or 5 %, respectively. For eGFP images the pinhole was adjusted to 100.5 AU (12.11 µm), and for mKO2 the pinhole was set to 115.4 AU (18.54 µM), while no emission filter was used. The detection range was set to 500-550 nm for the eGFP fluorescence and 560-600 nm for the mKO2 fluorescence.

5.9. Test of over-expression

Following the transformation of BL21 Star™ (DE3) One Shot® cells, clones expressing the target FtsZ isoform were selected. The pLATE31-Cm plasmid, encoding a C-terminal His-tagged chloramphenicol acetyltransferase was used as a control. Non-induced samples served as negative controls. Bacteria were cultured at 37 °C in LB medium with 50 mg/ml ampicillin and 1 % glucose. After overnight growth, 2.8 mL of fresh LB/amp was inoculated with 200 µL of the culture, and cells were incubated until an OD600 of ~0.5 (3 h). Protein expression was induced with 0.5 mM IPTG for 3 h. Cell pellets were harvested, frozen at -20 °C, thawed on ice, and resuspended in 200 µL HEPES NaOH pH 7.5 with 2 % SDS. Samples were incubated for 5 min at 95 °C, centrifuged at 13,000 rpm for 5 min, and supernatants were used for SDS-PAGE and western blot analysis. Proteins were transferred to a polyvinylidene fluoride (PVDF) membrane (Amersham, Cytiva, Marlborough, USA) using a Trans-Blot® SD Semi-Dry Transfer Cell (Bio-Rad) for 1.5 h at 1.5 mA/cm^2. Unspecific binding sites on the membrane were blocked for 1 h at room temperature using 4 % ECL blocking powder (Amersham™ ECL™ Blocking Agent, Cytiva) in TBST. Immunodetections were performed with an anti-His antibody (anti-6X His tag® antibody ab18184, Abcam, 1:1,000). The anti-mouse antibody from sheep coupled to horseradish peroxidase was used as a secondary antibody (NA931, Cytiva) in a dilution of 1:50,000 in TBST 2 % ECL blocking powder. Detection was initiated using the ECL™ Prime Western Blotting Detection Reagent (RPN2236, Cytiva) following the manufacturer's instructions.

5.10. Overexpression and purification of C-terminal His-tagged FtsZ1-2, C-terminal His-tagged FtsZ2-1 and his-tagged chloramphenicol transferase

Selected clones were cultured overnight at 37 °C in 200 mL LB medium containing 50 mg/mL ampicillin (amp) and 1 % glucose. 42 mL of the overnight culture was used to inoculate 558 mL of fresh LB/amp, and incubated at 37 °C until the OD600 reached ~0.5 (2.5 h). Expression was induced by addition of IPTG to a final concentration of 0.5 mM. After 3 h, cells were harvested by centrifugation at 5500 rpm and 4 °C, and the pellets were frozen at -20 °C. For further analysis, pellets were thawed on ice and resuspended in binding buffer (50 mM Tris HCl pH 7.5, 0.5 M NaCl, and 20 mM imidazole) with lysozyme (1 mg/mL, Sigma) and protease inhibitor cocktail (1 tablet / 50 mL cOmplete™, EDTA-free protease inhibitor cocktail, Roche). Cell lysis was performed twice using a sonicator (Q500 Sonicator®, QSonica Sonicators) for 5 min at 50 % amplitude on a 20 sec on, 45 sec off cycle. Cell debris was removed by centrifugation for 30 min at 15,000 rpm at 4 °C. The supernatants were transferred to fresh tubes and filtrated first through a 5 µm syringe PES filter (CHROMAFIL® Xtra PES, 5.0 µm, Macherey-Nagel), then through a 1 µm (Whatman™ Puradisc, Cytiva), and then through 0.22 µm (ROTILABO®, Roth). The filtrates were further purified by nickel affinity chromatography using buffers containing 50 mM Tris HCl pH 7.5, 0.5 M NaCl, and 20 mM imidazole for binding or 500 mM imidazole for elution (EB), respectively. The filtrate was loaded onto a 5 mL HisTrap FF column coupled with the ÄKTA start system (Cytiva). The elution of moss FtsZ was achieved using stepwise elution for the respective FtsZ isoform. For purification of FtsZ1-2_His_8, the column was washed with 38 column volumes (CV) of binding buffer. The protein was then eluted using a stepwise gradient (5 % EB for 10 CV, 15 % EB for 8 CV, 27 % EB for 7 CV, 33 % EB for 2 CV, 75 % EB for 5 CV, 100 % EB for 3 CV) and collected in 5 mL fractions. The last two fractions obtained with 75 % elution buffer were pooled. For purification of FtsZ2-1_His_8, the column was also eluted stepwise (6 % EB for 9 CV, 17 % EB for 11 CV, 38 % EB for 5 CV, 79 % EB for 4 CV, 100 % EB for 2 CV) and collected in 5 mL fractions. The last two fractions obtained with 79 % elution buffer were pooled. Fractions containing purified FtsZ1-2_His_8 and FtsZ2-1_His_8 were dialyzed against low salt buffer (LSB, adapted from Porter et al., 2021, 50 mM Tris HCl, pH 7.5, 0.5 M NaCl, 5 % Glycerol) using Slide-A-Lyzer® MINI Dialysis Devices, 20 K MWCO (Thermo Fisher Scientific). Proteins were concentrated using Pierce™ Protein Concentrators PES, 10 kDa MWCO (PES membrane, 20 mL, Thermo Fisher Scientific). FtsZ1-2 and FtsZ2-1 yields after purification were quantified via densitometry after SDS-PAGE using BSA as protein standard. The amount of FtsZ was calculated based on the intensity of the protein standard using GelAnalyzer 19.1 (www.gelanalyzer.com).

5.11. Overexpression and purification of His_6_SUMO_FtsZ1-2 and His_6_SUMO_FtsZ2-1

For the purification of His_6_SUMO_FtsZ1-2 and His_6_SUMO_FtsZ2-1, BL21 Star™ (DE3) One Shot® (Invitrogen, Thermo Fisher Scientific) cells were transformed with the respective vectors and the transformed cells were used to inoculate 200 mL LB medium containing 50 mg/ml kanamycin and

0.025 % glucose. Cultures were grown overnight at 37 °C and used to inoculate 500 mL of a simplified version of autoinduction media (derived from Studier, 2014) to an OD_{600} of 0.025. The simplified version of the autoinduction media contained 25 mM phosphate buffer pH 7.4, tryptone (20 g/L), yeast extract (5 g/L), 85 mM NaCl, 60 % glycerol (v/v), 10 % glucose (w/v), and 8 % lactose (w/v). This culture was incubated at 37 °C until it reached an OD_{600} of ~1.0 (2.5 h). The temperature was immediately lowered to 25 °C, and growth was continued overnight. On the next day, the OD_{600} was measured every hour until the OD_{600} did not change for 2 h. Cells were harvested by centrifugation at 5,500 rpm in an SS-34 rotor at 4 °C, and the pellets were frozen at -20 °C. For further analysis, the pellets were thawed on ice and resuspended in binding buffer containing 50 mM Tris HCl pH 8.5, 0.25 M NaCl, 1 mM $MgCl_2$, and 20 mM imidazole. The cell lysis was performed by sonification as described above and repeated twice. Cell debris was removed by centrifugation for 30 min in an SS-34 rotor at 15,000 x g at 4 °C. After cell lysis, the recombinant FtsZ proteins were purified by nickel affinity chromatography. The supernatant was loaded onto a 5 mL HisTrap FF column (Cytiva) coupled with the ÄKTA Purifier system (Cytiva) at a flow rate of 0.7 mL/min. For purification of His_6_SUMO_FtsZ1-2 the column was first washed with binding buffer using 50 mM of imidazole and the proteins were eluted in buffer with 500 mM imidazole. For purification of His_6_SUMO_FtsZ2-1 the column was first washed with binding buffer containing 25 mM of imidazole and the proteins were eluted in buffer with 250 mM imidazole. Elution fractions were collected and the protein-containing fractions were pooled. The His_6-SUMO tag was removed by SUMO-protease cleavage. For the cleavage, the pH of the pooled fractions was at 8.5 and 9.5 for FtsZ1-2 and FtsZ2-1, respectively. Cleavage was performed overnight at 4 °C using 20 ng/mL His-Ulp1 protease (SUMO-protease) in the presence of 2 mM DTT, 0.1 % ND-40, 200 µM GDP, and 1 mM $MgCl_2$. SUMO protease was produced in-house (Lau et al., 2018; Nußbaum et al., 2023). Following the removal of the His_6_SUMO-tag, the pH was increased to pH 10 for FtsZ1-2, and kept at 9.5 for FtsZ2-1. Proteins were concentrated using Pierce™ Protein Concentrators PES, 10 kDa MWCO (PES membrane, 5 20 mL, Thermo Fisher Scientific). Finally, the cleaved proteins were applied to a HiLoad® 16/600 Superdex® 200 pg (Cytiva) size exclusion column equilibrated with 25 mM glycine pH 10.6, 50 mM NaCl, 1 mM $MgCl_2$, 5 % glycerol or 50 mM glycine pH 9.5, 250 mM NaCl, 1 mM $MgCl_2$, 5 % glycerol for FtsZ1-2 and FtsZ2-1, respectively. After gel filtration, protein concentrations of fractions containing FtsZ1-2 and FtsZ2-1 were determined using the Pierce BCA Protein Assay Kit (Thermo Fisher Scientific) according to the manufacturer's instructions.

5.12. Analytical gel filtration

Experiments were performed on a Superdex® 200 pg 10/300 GL (Cytiva) size exclusion column equilibrated with 25 mM glycine pH 10.6, 50 mM NaCl, 1 mM $MgCl_2$, 5 % glycerol and 50 mM glycine pH 9.5, 250 mM NaCl, 1 mM $MgCl_2$, 5 % glycerol for FtsZ1-2 and FtsZ2-1, respectively. The

column was calibrated with gamma-globulin (158 kDa), ovalbumin (44 kDa), myoglobin (17.1 kDa) and vitamin B12 (1.35 kDa).

5.13. Protein buffer exchange

Buffer exchange was performed on a HiPrep™ 26/10 Desalting (Cytiva) size exclusion column equilibrated with 25 mM glycine pH 10.6, 50 mM KCl, 1 mM $MgCl_2$, 5 % glycerol and 50 mM glycine pH 9.5, 250 mM KCl, 1 mM $MgCl_2$, 5 % glycerol for FtsZ1-2 and FtsZ2-1, respectively.

5.14. GTP hydrolysis assay

The GTPase assay was performed to show FtsZ activity *in vitro*. The assay was a colorimetric assay and was performed in two 96-well plates. Final experiments were performed in the following buffers: 25 mM glycine pH 10.6, 50 mM KCl, 1 mM $MgCl_2$, 5 % glycerol and 50 mM glycine pH 9.5, 250 mM KCl, 1 mM $MgCl_2$, 5 % glycerol for FtsZ1-2 and FtsZ2-1, respectively. The 10 mM GTP stock solution as well as the 0 - 40 mM phosphate standard dilution were prepared in the respective protein buffer. The required concentration of FtsZ (2 µM, 5 µM, 7.5 µM, 10 µM, and 15 µM) was prepared in protein buffer in a total volume of 20 µL per reaction. The assay was performed at 25 °C. After initiation of the reaction with 1 mM GTP, the reaction was stopped at various time points using 20 mM EDTA. 20 µL aliquots of malachite green (Malachite Green Phosphate Assay Kit, Sigma-Aldrich) working reagent were added in a second 96-well plate (Greiner Bio One) and 60 µL of protein buffer were added. The colour formation was measured on a plate reader (CLARIOstar® Plus, BMG LABTECH GmbH, Ortenberg, Germany) at 600 nm and the amount of free phosphate in every sample was calculated based on the phosphate standard calibration curve. The design of the graphs was performed using GraphPad Prism version 10.1.0 (316) for Windows, GraphPad Software, Boston, Massachusetts USA, www.graphpad.com.

5.15. Light Scattering Assays (LSA)

Light Scattering Assays to analyse *in vitro*-polymerization were performed on a FluoroMax-4 spectrofluorometer (Horiba Scientific). Assays were performed in a wide variety of buffers to optimize filament formation. The proteins were centrifuged prior to the experiments. The following parameters were used: emission and the excitation wavelengths were both set at 350 nm with both slit widths set to 0.5 nm and. After 50 sec, 1 mM GTP was added to 15 µM FtsZ and the reaction was observed for 10 min.

5.16. Transmission electron microscopy of FtsZ filaments

For polymerization studies, FtsZ proteins were incubated for 5 min with 2 mM GTP at room temperature. 15 µM of purified FtsZ with and without GTP were applied on freshly glow-discharged

carbon/Formvar-coated copper grids (300 mesh; Plano GmbH) and incubated for 30 sec. The excess liquid was blotted away and the grid was washed three times with ddH_2O, followed by negative staining with 2 % uranyl acetate. Images were taken with a Hitachi HT7800 operated at 100 kV, equipped with an EMSIS Xarosa 20-megapixel CMOS camera.

6. References

Asgharzadeh P, Özdemir B, Reski R, Röhrle O, Birkhold AI (2018) Computational 3D imaging to quantify structural components and assembly of protein networks. Acta Biomaterialia 69: 206-217

Asgharzadeh P, Birkhold AI, Trivedi Z, Özdemir B, Reski R, Röhrle O (2020) A NanoFE simulation-based surrogate machine learning model to predict mechanical functionality of protein networks from live confocal imaging. Computational and Structural Biotechnology Journal 18: 2774-2788

Barrows JM, Goley ED. (2021) FtsZ dynamics in bacterial division: What, how, and why? Current Opinion in Cell Biology 68: 163-172

Betz O, Birkhold A, Caliaro M, Eggs B, Mader A, Knippers J, Röhrle O, Speck O (2016) Adaptive stiffness and joint-free kinematics: Actively actuated rod-shaped structures in plants and animals and their biomimetic potential in architecture and engineering. Biomimetic Research for Architecture and Building Construction: Biological Design and Integrative Structures 9: 135-167

Bi E, Lutkenhaus J (1991) FtsZ ring structure associated with division in *Escherichia coli*. Nature 354: 161–164

Bisson-Filho AW, Hsu Y-P, Squyres GR, Kuru E, Wu F, Jukes C, Sun Y, Dekker C, Holden S, VanNieuwenhze MS, Brun YV., Garner EC (2017) Treadmilling by FtsZ filaments drives peptidoglycan synthesis and bacterial cell division. Science 355: 739–743

de Boer P, Crossley R, Rothfield L (1992) The essential bacterial cell-division protein FtsZ is a GTPase. Nature 359: 254–256

Cox J, Hein MY, Luber CA, Paron I, Nagaraj N, Mann M (2014) Accurate proteome-wide label-free quantification by delayed normalization and maximal peptide ratio extraction, termed MaxLFQ. Molecular & Cellular Proteomics 13: 2513–2526

Cox J, Mann M (2008) MaxQuant enables high peptide identification rates, individualized p.p.b.-range mass accuracies and proteome-wide protein quantification. Nature Biotechnology 26: 1367–1372

Dai K, Lutkenhaus J (1991) *ftsZ* is an essential cell division gene in *Escherichia coli*. Journal of Bacteriology 173: 3500–3506

Erickson HP (1995) FtsZ, a prokaryotic homolog of tubulin? Cell 80: 367–370

Erickson HP, Anderson DE, Osawa M (2010) FtsZ in bacterial cytokinesis: Cytoskeleton and force generator all in one. Microbiology and Molecular Biology Reviews 74: 504-528

Gibson DG, Young L, Chuang R-Y, Venter JC, Hutchison CA, Smith HO (2009) Enzymatic assembly of DNA molecules up to several hundred kilobases. Nature Methods 6: 343–345

Gould SB, Waller RF, McFadden GI (2008) Plastid evolution. Annual Review of Plant Biology 59: 491–517.

Gremillon L, Kiessling J, Hause B, Decker EL, Reski R, Sarnighausen E (2007) Filamentous temperature-sensitive Z (FtsZ) isoforms specifically interact in the chloroplasts and in the cytosol of *Physcomitrella patens*. New Phytologist 176: 299–310

Grosche C, Rensing SA (2017) Three rings for the evolution of plastid shape: a tale of land plant FtsZ. Protoplasma 254: 1879–1885

Hirano T, Tanidokoro K, Shimizu Y, Kawarabayasi Y, Ohshima T, Sato M, Tadano S, Ishikawa H, Takio S, Takechi K, Takano H. (2016) Moss chloroplasts are surrounded by a peptidoglycan wall containing D-amino acids. Plant Cell 28: 1521-1532

Hoernstein SNW, Özdemir B, van Gessel N, Miniera AA, Rogalla von Bieberstein B, Nilges L, Schweikert Farinha J, Komoll R, Glauz S, Weckerle T, Scherzinger F, Rodriguez-Franco M, Müller-Schüssele SJ, Reski R (2023). A deeply conserved protease, acylamino acid-releasing enzyme (AARE), acts in ageing in Physcomitrella and Arabidopsis. Communications Biology 6: 61

Hohe A, Reski R (2002) Optimisation of a bioreactor culture of the moss *Physcomitrella patens* for mass production of protoplasts. Plant Science 163: 69–74

Hohe A, Egener T, Lucht JM, Holtorf H, Reinhard C, Schween G, Reski R. (2004) An improved and highly standardised transformation procedure allows efficient production of single and multiple targeted gene-knockouts in a moss, *Physcomitrella patens*. Current Genetics 44: 339-347

Howell M, Aliashkevich A, Sundararajan K, Daniel JJ, Lariviere PJ, Goley ED, Cava F, Brown PJB (2019) *Agrobacterium tumefaciens* divisome proteins regulate the transition from polar growth to cell division. Molecular Microbiology 111: 1074–1092

Ithurbide S, Gribaldo S, Albers S-V, Pende N (2022) Spotlight on FtsZ-based cell division in Archaea. Trends in Microbiology 30: 665-678

Jost W, Link S, Horstmann V, Decker EL, Reski R, Gorr G (2005) Isolation and characterization of three moss-derived beta-tubulin promoters suitable for recombinant expression. Current Genetics 47: 111-120

Kalyan BGP, Kumar L (2022) 3D printing: Applications in tissue engineering, medical devices, and drug delivery. AAPS PharmSciTech. 23: 92

Kasten B, Reski R (1997) beta-lactam antibiotics inhibit chloroplast division in a moss (*Physcomitrella patens*) but not in tomato (*Lycopersicon esculentum*). Journal of Plant Physiology 150: 137-140

Keeling PJ (2013) The number, speed, and impact of plastid endosymbioses in eukaryotic evolution. Annual Review of Plant Biology 64: 583–607

Khraiwesh B, Ossowski S, Weigel D, Reski R, Frank W (2008) Specific gene silencing by artificial microRNAs in *Physcomitrella patens*: An alternative to targeted gene knockouts. Plant Physiology 148: 684-693

Kiessling J, Kruse S, Rensing SA, Harter K, Decker EL, Reski R (2000) Visualization of a cytoskeleton-like FtsZ network in chloroplasts. Journal of Cell Biology 151: 945–950

Kiessling J, Martin A, Gremillon L, Rensing SA, Nick P, Sarnighausen E, Decker EL, Reski R (2004) Dual targeting of plastid division protein FtsZ to chloroplasts and the cytoplasm. EMBO Reports 5: 889-894

Köhler RH, Cao J, Zipfel WR, Webb WW, Hanson MR (1997) Exchange of protein molecules through connections between higher plant plastids. Science 276: 2039-2042

Król E, Scheffers D-J (2013) FtsZ polymerization assays: Simple protocols and considerations. Journal of Visualized Experiments 81: 50844

Lang D, Ullrich KK, Murat F, Fuchs J, Jenkins J, Haas FB, Piednoel M, Gundlach H, Van Bel M, Meyberg R, Vives C, Morata J, Symeonidi A, Hiss M, Muchero W, Kamisugi Y, Saleh O, Blanc G, Decker EL, van Gessel N, Grimwood J, Hayes RD, Graham SW, Gunter LE, McDaniel SF, Hoernstein SNW, Larsson A, Li FW, Perroud PF, Phillips J, Ranjan P, Rokshar DS, Rothfels CJ, Schneider L, Shu S, Stevenson DW, Thümmler F, Tillich M, Villarreal Aguilar JC, Widiez T, Wong GK, Wymore A, Zhang Y, Zimmer AD, Quatrano RS, Mayer KFX, Goodstein D, Casacuberta JM, Vandepoele K, Reski R, Cuming AC, Tuskan GA, Maumus F, Salse J, Schmutz J, Rensing SA (2018) The *Physcomitrella patens* chromosome-scale assembly reveals moss genome structure and evolution. Plant Journal 93: 515-533

Lau YK, Baytshtok V, Howard TA, Fiala BM, Johnson JM, Carter LP, Baker D, Lima CD, Bahl CD (2018) Discovery and engineering of enhanced SUMO protease enzymes. Journal of Biological Chemistry 293: 13224-13233

Leister D (2019) Genetic engineering, synthetic biology and the light reactions of photosynthesis. Plant Physiology 179: 778–793

Loose M, Mitchison TJ (2014) The bacterial cell division proteins FtsA and FtsZ self-organize into dynamic cytoskeletal patterns. Nature Cell Biology 16: 38-46

Liao Y, Ithurbide S, Evenhuis C, Löwe J, Duggin IG (2021) Cell division in the archaeon *Haloferax volcanii* relies on two FtsZ proteins with distinct functions in division ring assembly and constriction. Nature Microbiology 6: 594-605

Liu X, An J, Wang L, Sun Q, An C, Wu B, Hong C, Wang X, Dong S, Guo J, Feng Y, Gao H (2022) A novel amphiphilic motif at the C-terminus of FtsZ1 facilitates chloroplast division. Plant Cell 34: 419-432

Löwe J, Amos LA (1998) Crystal structure of the bacterial cell-division protein FtsZ. Nature 391: 203–206

Lutkenhaus J, Addinall SG (1997) Bacterial cell division and the Z ring. Annual Review of Biochemistry 66: 93-116

Lutkenhaus JF, Wolf-Watz H, Donachie WD (1980) Organization of genes in the ftsA-envA region of the *Escherichia coli* genetic map and identification of a new fts locus (ftsZ). Journal of Bacteriology 142: 615–620

Ma X, Ehrhardt DW, Margolin W (1996) Colocalization of cell division proteins FtsZ and FtsA to cytoskeletal structures in living *Escherichia coli* cells by using green fluorescent protein. Proceedings of the National Academy of Sciences USA 93: 12998–13003

Martin A, Lang D, Heckmann J, Zimmer AD, Vervliet-Scheebaum M, Reski R (2009a): A uniquely high number of ftsZ genes in the moss *Physcomitrella patens*. Plant Biology 11: 744-750

Martin A, Lang D, Hanke ST, Mueller SJX, Sarnighausen E, Vervliet-Scheebaum M, Reski R (2009b) Targeted gene knockouts reveal overlapping functions of the five *Physcomitrella patens* FtsZ isoforms in chloroplast division, chloroplast shaping, cell patterning, plant development, and gravity sensing. Molecular Plant 2: 1359–1372

Martin W, Stoebe B, Goremykin V, Hansmann S, Hasegawa M, Kowallik KV (1998) Gene transfer to the nucleus and the evolution of chloroplasts. Nature 393: 162–165

MacLeod AI, Knopp MR, Gould SB (2023) A mysterious cloak: the peptidoglycan layer of algal and plant plastids. Protoplasma 261: 173-178

McFadden GI (1999) Endosymbiosis and evolution of the plant cell. Current Opinion in Plant Biology 2: 513–519

Miyagishima S, Nozaki H, Nishida K, Nishida K, Matsuzaki M, Kuroiwa T (2004) Two types of FtsZ proteins in mitochondria and red-lineage chloroplasts: The duplication of FtsZ is implicated in endosymbiosis. Journal of Molecular Evolution 58: 291–303

Mueller SJ, Lang D, Hoernstein SN, Lang EG, Schuessele C, Schmidt A, Fluck M, Leisibach D, Niegl C, Zimmer AD, Schlosser A, Reski R (2014) Quantitative analysis of the mitochondrial and plastid proteomes of the moss *Physcomitrella patens* reveals protein macrocompartmentation and microcompartmentation. Plant Physiology 164: 2081-2095

Mukherjee A, Lutkenhaus J (1998) Dynamic assembly of FtsZ regulated by GTP hydrolysis. EMBO Journal 17: 462-469

Mukherjee A, Lutkenhaus J (1999) Analysis of FtsZ assembly by light scattering and determination of the role of divalent metal cations. Journal of Bacteriology 181: 823–832

Mukherjee A, Dai K, Lutkenhaus J (1993) *Escherichia coli* cell division protein FtsZ is a guanine nucleotide binding protein. Proceedings of the National Academy of Sciences USA 90: 1053-1057

Nußbaum P, Kureisaite-Ciziene D, Bellini D, van der Does C, Kojic M, Taib N, Gribaldo S, Loose M, Löwe J, Albers SV (2023) PRC domain-containing proteins modulate FtsZ-based archaeal cell division. bioRxiv doi: https://doi.org/10.1101/2023.03.28.534543

Okazaki K, Kabeya Y, Miyagishima SY (2010) The evolution of the regulatory mechanism of chloroplast division. Plant Signaling & Behavior 5: 164-167

Okazaki K, Kabeya Y, Suzuki K, Mori T, Ichikawa T, Matsui M, Nakanishi H, Miyagishima SY (2009) The PLASTID DIVISION1 and 2 components of the chloroplast division machinery determine the rate of chloroplast division in land plant cell differentiation. Plant Cell 21: 1769-1780

Olson BJSC, Wang Q, Osteryoung KW (2010) GTP-dependent heteropolymer formation and bundling of chloroplast FtsZ1 and FtsZ2. Journal of Biological Chemistry 285: 20634–20643

Osteryoung KW, McAndrew RS (2001) The plastid division machine. Annual Review of Plant Physiology and Plant Molecular Biology 52: 315-333

Osteryoung KW, Nunnari J (2003) The division of endosymbiotic organelles. Science 302: 1698-1704

Osteryoung KW, Vierling E (1995) Conserved cell and organelle division. Nature 376: 473–474

Osteryoung KW, Stokes KD, Rutherford SM, Percival AL, Lee WY (1998) Chloroplast division in higher plants requires members of two functionally divergent gene families with homology to bacterial *ftsZ*. Plant Cell 10: 1991–2004

Özdemir B, Reski R (2021) Automated and semi-automated enhancement, segmentation and tracing of cytoskeletal networks in microscopic images: A review. Computational and Structural Biotechnology Journal 19: 2106-2120

Özdemir B, Asgharzadeh P, Birkhold AI, Mueller SJ, Röhrle O, Reski R (2018) Cytological analysis and structural quantification of FtsZ1-2 and FtsZ2-1 network characteristics in *Physcomitrella patens*. Scientific Reports 8: 11165

Özdemir B, Asgharzadeh P, Birkhold A, Röhrle O, Reski R (2019) The plastid skeleton: a source of ideas in the nano range. Biomimetics for Architecture: Learning from Nature: 163-166

Porter KJ, Cao L, Chen Y, TerBush AD, Chen C, Erickson HP, Osteryoung KW (2021) The *Arabidopsis thaliana* chloroplast division protein FtsZ1 counterbalances FtsZ2 filament stability *in vitro*. Journal of Biological Chemistry 296: 100627

Porter KJ, Cao L, Osteryoung KW (2023) Dynamics of the *Synechococcus elongatus* cytoskeletal GTPase FtsZ yields mechanistic and evolutionary insight into cyanobacterial and chloroplast FtsZs. Journal of Biological Chemistry 299: 102917

Rensing SA, Kiessling J, Reski R, Decker EL (2004) Diversification of ftsZ during early land plant evolution. Journal of Molecular Evolution 58: 154–162

Reski R (2002) Rings and networks: the amazing complexity of FtsZ in chloroplasts. Trends in Plant Science 7: 103-105

Reski R (2009) Challenges to our current view on chloroplasts. Biological Chemistry 390: 731-738

Sambrook J, Russell DW (2006) Standard ethanol precipitation of DNA in microcentrifuge tubes. Cold Spring Harbor Protocols 2006: pdb.prot4456

Santana-Molina C, del Saz-Navarro D, Devos DP (2023) Early origin and evolution of the FtsZ/tubulin protein family. Frontiers in Microbiology 13: 1100249

Schwanhäusser B, Busse D, Li N, Dittmar G, Schuchhardt J, Wolf J, Chen W, Selbach M (2011) Global quantification of mammalian gene expression control. Nature 473: 337-342

Shih YL, Rothfield L (2006) The bacterial cytoskeleton. Microbiology and Molecular Biology Reviews 70: 729-754

Silhavy TJ, Kahne D, Walker S (2010) The bacterial cell envelope. Cold Spring Harbor Perspectives in Biology 2: a000414

Smith AG, Johnson CB, Vitha S, Holzenburg A (2010) Plant FtsZ1 and FtsZ2 expressed in a eukaryotic host: GTPase activity and self-assembly. FEBS Letters 584: 166–172

Suppanz I, Sarnighausen E, Reski R (2007) An integrated physiological and genetic approach to the dynamics of FtsZ targeting and organisation in a moss, *Physcomitrella patens*. Protoplasma 232: 1-9

Strepp R, Scholz S, Kruse S, Speth V, Reski R (1998) Plant nuclear gene knockout reveals a role in plastid division for the homolog of the bacterial cell division protein FtsZ, an ancestral tubulin. Proceedings of the National Academy of Sciences USA 95: 4368–4373

Studier FW (2014) Stable expression clones and auto-induction for protein production in *E. coli*. Methods in Molecular Biology 1091: 17-32

te Brinke E, Groen J, Herrmann A, Heus HA, Rivas G, Spruijt E, Huck WTS (2018) Dissipative adaptation in driven self-assembly leading to self-dividing fibrils. Nature Nanotechnology 13: 849-855

TerBush AD, Yoshida Y, Osteryoung KW (2013) FtsZ in chloroplast division: structure, function and evolution. Current Opinion in Cell Biology 25: 461–470

TerBush AD, Porzondek CA, Osteryoung KW (2016) Functional analysis of the chloroplast division complex using *Schizosaccharomyces pombe* as a heterologous expression system. Microscopy and Microanalysis 22: 275–289

Tian GW, Mohanty A, Chary SN, Li S, Paap B, Drakakaki G, Kopec CD, Li J, Ehrhardt D, Jackson D, Rhee SY, Raikhel NV, Citovsky V (2004) High-throughput fluorescent tagging of full-length Arabidopsis gene products *in planta*. Plant Physiology 135: 25-38

Top O, Milferstaedt SWL, van Gessel N, Hoernstein SNW, Özdemir B, Decker EL, Reski R (2021) Expression of a human cDNA in moss results in spliced mRNAs and fragmentary protein isoforms. Communications Biology 4: 964

Tyanova S, Temu T, Sinitcyn P, Carlson A, Hein MY, Geiger T, Mann M, Cox J (2016) The Perseus computational platform for comprehensive analysis of (prote)omics data. Nature Methods 13: 731–740

Vitha S, McAndrew RS, Osteryoung KW (2001) FtsZ ring formation at the chloroplast division site in plants. Journal of Cell Biology 153: 111–119

Wagstaff J, Löwe J (2018) Prokaryotic cytoskeletons: protein filaments organizing small cells. Nature Reviews Microbiology 16: 187-201

Wall L, Christiansen T, Orwant J (2000) Programming Perl, 3rd ed. O'Reilly, Beijing; Cambridge, Mass

Ward JE Jr, Lutkenhaus J (1985) Overproduction of FtsZ induces minicell formation in *E. coli*. Cell 42: 941-949

Waterhouse AM, Procter JB, Martin DMA, Clamp M, Barton GJ (2009) Jalview Version 2—a multiple sequence alignment editor and analysis workbench. Bioinformatics 25: 1189–1191

Wiedemann G, van Gessel N, Köchl F, Hunn L, Schulze K, Maloukh L, Nogué F, Decker EL, Hartung F, Reski R (2018) RecQ helicases function in development, DNA repair and gene targeting in *Physcomitrella patens*. Plant Cell 30: 717-736

Yang X, Lyu Z, Miguel A, McQuillen R, Huang KC, Xiao J (2017) GTPase activity–coupled treadmilling of the bacterial tubulin FtsZ organizes septal cell wall synthesis. Science 355: 744–747

Yoshida Y, Mogi Y, TerBush AD, Osteryoung KW (2016) Chloroplast FtsZ assembles into a contractible ring via tubulin-like heteropolymerization. Nature Plants 2: 16095

Zhang Y, Wen Z, Washburn MP, Florens L (2010) Refinements to label free proteome quantitation: How to deal with peptides shared by multiple proteins. Analytical Chemistry 82: 2272–2281

Zimorski V, Ku C, Martin WF, Gould SB (2014) Endosymbiotic theory for organelle origins. Current Opinion in Microbiology 22: 38–48

Zupan JR, Cameron TA, Anderson-Furgeson J, Zambryski PC (2013) Dynamic FtsA and FtsZ localization and outer membrane alterations during polar growth and cell division in *Agrobacterium tumefaciens*. Proceedings of the National Academy of Sciences USA 110: 9060–9065

7. Acknowledgements

This project was funded by the German Research Foundation DFG under Germany's Excellence Strategy (*liv*MatS - EXC-2193/1, Project ID 390951807, and CIBSS – EXC-2189, Project ID 390939984) to R.R. S.W.L.M. was supported by a state-funded completion scholarship of the Landesgraduiertenförderung LGFG. M.J. was supported by a grant to Sonja-Verena Albers by the Collaborative Research Centre SFB1381 funded by the DFG-Project-ID 403222702-SFB 1381. The TEM (Hitachi HT7800) was funded by the DFG grant (project number 426849454) and is operated by the University of Freiburg, Faculty of Biology, as a partner unit within the Microscopy and Image Analysis Platform (MIAP) and the Life Imaging Center (LIC), Freiburg.

We thank Dr. Oğuz Top for codon optimizing the CDS of Physcomitrella FtsZ1-2 and FtsZ2-1 for bacterial expression. We also thank the Life Imaging Center (LIC) of the University of Freiburg for help with confocal microscopy. We thank Sonja-Verena Albers for providing the equipment for purification of Physcomitrella FtsZ proteins and her overall support of this project, and Anne Katrin Prowse for language editing.

8. Author contributions

S.W.L.M. designed the research, performed the experiments, analysed the data, and wrote the manuscript. M.J. performed transmission electron microscopy. S.N.W.H. performed quantitative Co-IPs, analysis of MS data and helped writing the manuscript. L.L.B. performed confocal microscopy and helped writing the manuscript. B.Ö. generated the FtsZ2-1-eGFP fusion line. C.v.d.D. helped with designing and performing the experiments, analysed data and helped writing the manuscript. E.L.D. helped writing the manuscript. R.R. designed and supervised the research, acquired funding, and wrote the manuscript. All authors read and approved the final version of the manuscript.

Conflict of Interest

All authors declare no conflict of interest.

9. Supplemental Information

Table S1 Oligonucleotides and the respective template accessions or templates used for the generation of the FtsZ2-1-eGFP fusion construct.

Name	Sequence (5‘ to 3‘)	Sequence Accession
ftsZ2-1_5HR_Fwd	CGTCTCTCTCTGTTGGGCTTGTGAGGAA	Pp3c11_17860V3
ftsZ2-1_5HR_Rev	CTTGCTCACAGCTCCACCTCCACCTCCATGACGTGTCTGGCCTCGC	
Kin 2-1 3'HR Rev	ACTCTCGGCATGGACGAGCTGTACAAGTAAAGGTCGTAACATTGGAATTAC	
ftsZ2-1_3HR_Rev	CGTCTCAACATGTGTGATCCGTTTCG	
Link_GFP_F	GGAGGTGGAGGTGGAGCTAGTAAAGGAGAAGAACTTTTCAC	U70495.1
eGFP_Rev	GGCCCCAGCGGCCGCAGCAGCACCAGCCTTGTACAGCTCGTCCATGCC	U55763.1
FTSZ2_1_GFP_5int_fwd	GCCACAGGGATAGTCTGGAA	Pp3c11_17860V3
FTSZ2_1_GFP_5int_rev	GAACTTCAGGGTCAGCTTGC	U55763.1
FTSZ2_1_GFP_3int_fwd	CGACCACTACCAGCAGAACA	U55763.1
FTSZ2_1_GFP_3int_rev	GTCTCACTGCGTCTTCGTCA	Pp3c11_17860V3

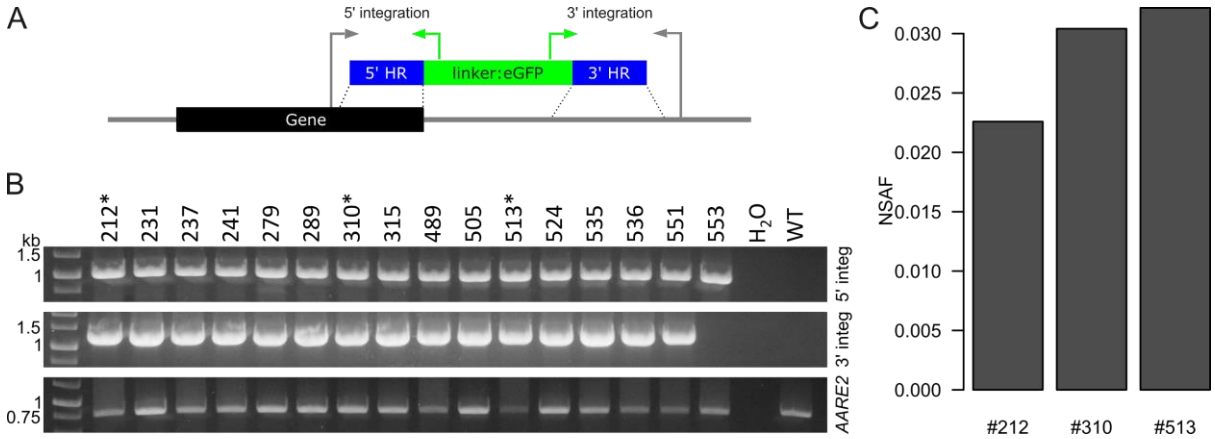

Figure S1 Identification of FtsZ2-1-GFP fusion lines *via* PCR and Co-immunoprecipitation (CoIP).

Primers were designed to represent correct positioning of the knock-in construct at the desired genomic locus (Pp3c11_17860V3). (A) Scheme representing the positioning of the knock-in construct and the primers used for the screening PCR. (B) Results of the screening PCR. Expected amplicon sizes: 5' integration: 1064 bp; 3' integration: 1302 bp; AARE2 (Pp3c12_21080V3): 768 bp. Stars (*) indicate candidate lines that were selected for a first test CoIP. (C) Results from the first test CoIP with selected FtsZ2.1:eGFP fusion lines. Relative quantitative share of FtsZ2.1:eGFP in the analysed sample is represented by normalized spectral abundance factors (NSAF, Zhang et al., 2010). A full spectrum report is available from Supplemental Table S2.

Table S2 List of proteins significantly interacting with Physcomitrella FtsZ2-1 as determined by Co-IP and subsequent MS analysis.

The list can be downloaded from Zenodo (DOI: 10.5281/zenodo.10648778).

Figure S2 Pairwise sequence alignment of Physcomitrella FtsZ1-2 (PpFtsZ1-2) and the codon optimized FtsZ1-2 (FtsZ1-2) for codon usage in *E. coli*. Alignment was performed with Jalview (Version 2.11.2.2, Waterhouse et al., 2009).

Figure S3 Pairwise sequence alignment of Physcomitrella FtsZ2-1 (PpFtsZ2-1) and the codon optimized FtsZ2-1 (FtsZ2-1) for codon usage in *E. coli*. Alignment was performed with Jalview (Version 2.11.2.2, Waterhouse et al., 2009).

Table S3 Oligonucleotides used for Ligation Independent Cloning in this work.
Due to the cloning strategy, all forward oligonucleotides (fwd) include the sequence 5' AGAAGGAGATATAACTATG 3' at their 5' end; all reverse oligonucleotides (rev) include the sequence 5' GGAGATGGGAAGTCATTA 3' at their 5' end.

Name	Sequence (5' to 3')
C1pLATE_optiFtsZ1-2_fwd	GCTGTTCGTGTTACCTCTCGTTGCC
C1optiFtsZ1-2_H_pLATE_rev	GTGGTGGTGGTGGTGGTGGTGGTGCAGGAAACCTTTACGGTTCAGACCCTG
C2pLATE_optieGFP_1-2_fwd	GTTTCTAAAGGTGAAGAACTGTTCACCGGTG
C2optiFtsZ1-2_H_pLATE_rev	GTGGTGGTGGTGGTGGTGGTGGTGCAGGAAACCTTTACGGTTCAGACCCTG
C3pLATE_H_optiFtsZ1-2_fwd	CACCACCACCACCACCACCACCACGTTCGTGTTACCTCTCGTTGCCGTT
C3optiFtsZ1-2_eGFP_pLATE_rev	TTTGTACAGTTCGTCCATACCCAGGGT
C4pLATE_H_optiFtsZ1-2_fwd	CACCACCACCACCACCACCACCACGTTCGTGTTACCTCTCGTTGCCGTT
C4optiFtsZ1-2_pLATE_rev	CAGGAAACCTTTACGGTTCAGACCCTG
C5pLATE_optieGFP_2-1_fwd	GTTTCTAAAGGTGAAGAACTGTTCACCGGTG
C5optiFtsZ2-1_H_pLATE_rev	GTGGTGGTGGTGGTGGTGGTGGTGGTGACGGGTCTGACCACGTTTACG
C6pLATE_optiFtsZ2-1_fwd	TCTATGCACTCTCGTTCTTCTGTTCG
C6optiFtsZ2-1_H_pLATE_rev	GTGGTGGTGGTGGTGGTGGTGGTGGTGACGGGTCTGACCACGTTTA
C7pLATE_H_optiFtsZ2-1_fwd	CACCACCACCACCACCACCACCACTCTATGCACTCTCGTTCTTCTGTTCGTGC
C7optiFtsZ2-1_eGFP_pLATE_rev	TTTGTACAGTTCGTCCATACCCAGGGTG
C8pLATE_H_optiFtsZ2-1_fwd	CACCACCACCACCACCACCACCACTCTATGCACTCTCGTTCTTCTGTTCGTGC
C8optiFtsZ2-1_pLATE_rev	GTGACGGGTCTGACCACGTTTACG
C9_mKO2_optiFtsZ2-1_pLATE_fwd	AGAAGGAGATATAACTATGGTGAGTGTGATTAAACCAGAGA
C9_mKO2_optiFtsZ2-1_pLATE_H_rev	GGAGATGGGAAGTCATTAGTGGTGGTGGTGGTGGTGGTGGTGGTGACGGGTCTGACCACG
C9_mKO2_H_pLATE_fwd	AGAAGGAGATATAACTATGGTGAGTGTGATTAAACCAGAGATG
C9_mKO2_H_pLATE_rev	GGAGATGGGAAGTCATTAGTGGTGGTGGTGGTGGTGGTGTGAATGAGCTACTGCATCTTCTACC

Table S4 Oligonucleotides used for Gibson cloning and sequencing in this work.

Name	Sequence (5' to 3')
pre3pJET_oFtsZ1-2_fwd	TCTTCCGGATGGCTCGAGTTTTTCAGCAAGATATGGTTCGTGTTACCTCTCGTTGCCGTT
pre3oFtsZ1-2_eGFP_rev	ACAACACCGGTGAACAGTTCTTCACCTTTAGAAACCAGGAAACCTTTACGGTTCAGACCCTG
pre3oFtsZ1-2_eGFP_fwd	TGTTCCGTCAGGGTCTGAACCGTAAAGGTTTCCTGGTTTCTAAAGGTGAAGAACTGTTCACCGGTG
pre37oeGFP_pJET_rev	TGAGAATATTGTAGGAGATCTTCTAGAAAGATTTATTTGTACAGTTCGTCCATACCCAGGGT
pre7pJET_oFtsZ2-1_fwd	TCTTCCGGATGGCTCGAGTTTTTCAGCAAGATATGTCTATGCACTCTCGTTCTTCTGTTCG
pre7oFtsZ1-2_eGFP_rev	ACAACACCGGTGAACAGTTCTTCACCTTTAGAAACGTGACGGGTCTGACCACGTTTA
pre7oFtsZ1-2_eGFP_fwd	CGTCTTTCCTGCGTAAACGTGGTCAGACCCGTCACGTTTCTAAAGGTGAAGAACTGTTCACCGGTG
pre2oeGFP_FtsZ1-2_rev	GCACCCAGCCAACGGCAACGAGAGGTAACACGAACTTTGTACAGTTCGTCCATACCCAGGGT
pre2oeGFP_FtsZ1-2_fwd	CTGGTATCACCCTGGGTATGGACGAACTGTACAAAGTTCGTGTTACCTCTCGTTGCCGTT
pre2oFtsZ1-2_pJET_rev	TGAGAATATTGTAGGAGATCTTCTAGAAAGATTTACAGGAAACCTTTACGGTTCAGACCCTG
pre25pJET_oeGFP_fwd	TCTTCCGGATGGCTCGAGTTTTTCAGCAAGATATGGTTTCTAAAGGTGAAGAACTGTTCACCGGTG
pre5oeGFP_FtsZ2-1_rev	CGCAGAGCACGAACAGAAGAACGAGAGTGCATAGATTTGTACAGTTCGTCCATACCCAGGGT
pre5oeGFP_FtsZ2-1_fwd	CTGGTATCACCCTGGGTATGGACGAACTGTACAAATCTATGCACTCTCGTTCTTCTGTTCG
pre5oFtsZ2-1_pJET_rev	CTGAGAATATTGTAGGAGATCTTCTAGAAAGATTTAGTGACGGGTCTGACCACGTTTA
SUMO_FtsZ1-2_fwd	GAAGCGCATCGCGAACAGATCGGTGGTATGGCTAACCTGTCTGGTGCTAAAATCAAAGTTATCGG
SUMO_FtsZ1-2_rev	CTCACTGCCCGCTTTCCAGTCGGGTCGACGGTTTACAGGAAACCTTTACGGTTCAGACCC
SUMO_FtsZ2-1_fwd	GAAGCGCATCGCGAACAGATCGGTGGTATGTCTCTGCGTCGTATCGACCGTGCTC
SUMO_FtsZ2-1_rev	CTCACTGCCCGCTTTCCAGTCGGGTCGACGGTTTAGTGACGGGTCTGACCACGTTTACGC
pre9_pJET_mKO2 _ oFtsZ2-1_fwd	GGATGGCTCGAGTTTTTCAGCAAGATATCATGGTGAGTGTGATTAAACCAGAGATG
pre9_pJET_mKO2 _ oFtsZ2-1_rev	CAGAAGAACGAGAGTGCATAGATGAATGAGCTACTGCATCTTCTACC
pre9oFtsZ2-1_mKO2_pJET_fwd	GTAGAAGATGCAGTAGCTCATTCATCTATGCACTCTCGTTCTTCTGTTC
pre9oFtsZ2-1_mKO2_pJET_rev	GTAGGAGATCTTCTAGAAAGATATCCTAGTGACGGGTCTGACCACG
mKO2_FtsZ21_eGFP_FtsZ12_fwd	GCAGATTGTACTGAGAGTGCACCAAATTGTGAGCGGATAACAATTTGAGCTC
mKO2_FtsZ21_eGFP_FtsZ12_rev	CTGTGCGGTATTTCACACCGCATACAAAAAACCCCTCAAGACCCGTT
SUMO_fwd	GCGTAGAGGATCGAGATCTCGATCCCG
T7_rev	GGGGTGCCTAATGAGTGAGCTAACTCAC

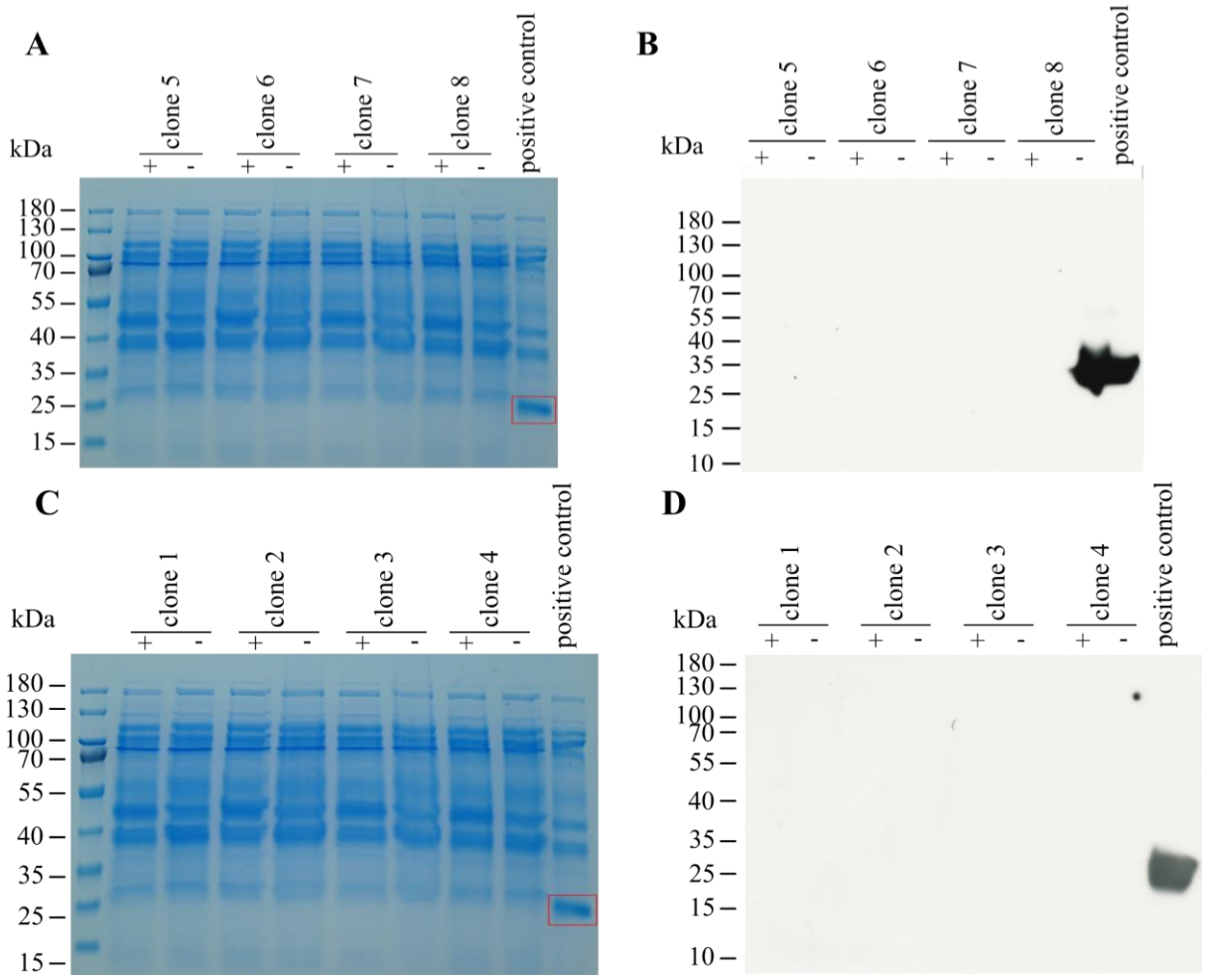

Figure S4 Coomassie-stained SDS gels and Immunoblot detection of BL21 Star™ (DE3) cells transformed with the pLATE11 expression vector for expression of Physcomitrella FtsZ1-2 and Physcomitrella FtsZ2-1 with N-terminal His-tags.

Total cell extracts of BL21 Star™ (DE3) cells transformed with the constructs for Physcomitrella FtsZ1-2 (A, B) and Physcomitrella FtsZ2-1 (C, D) were analysed by Coomassie-stained SDS-gels (A,C) and anti-His immunoblots (B,D). '+' and '-' signs indicate that the cells where either induced or not induced with IPTG. Red arrows indicate the overexpressed FtsZ1-2 and FtsZ2-1 proteins. The overexpression of His-tagged chloramphenicol acetyl transferase (red boxes) was used as a positive control.

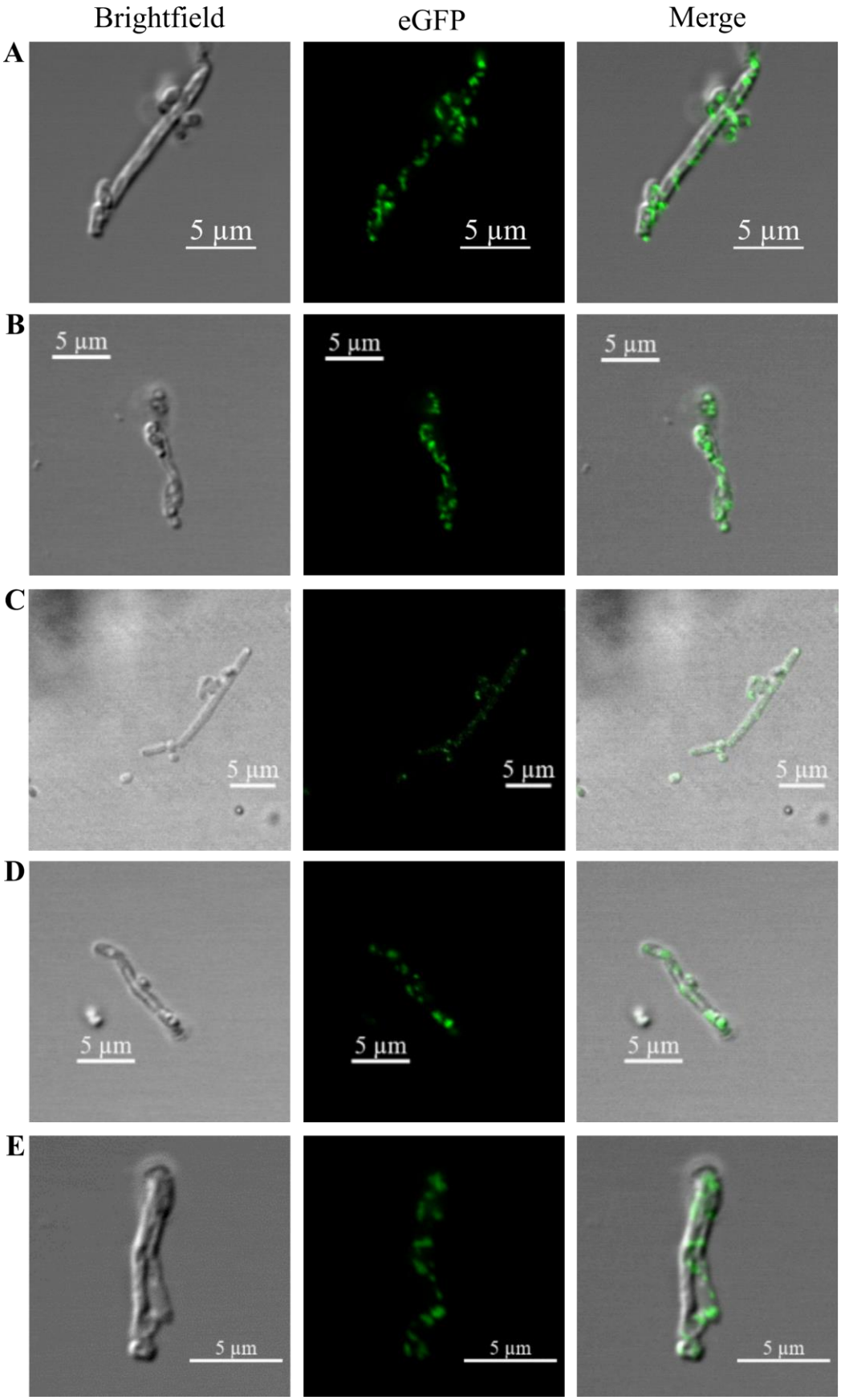

Figure S5 Confocal microscopy of eGFP-tagged Physcomitrella FtsZ1-2 in *E. coli*. BL21 Star™ (DE3) cells transformed with the constructs for eGFP-FtsZ1-2 were induced with 0.5 mM IPTG. Different elongated bacteria were observed (A-E). Scale bars as indicated.

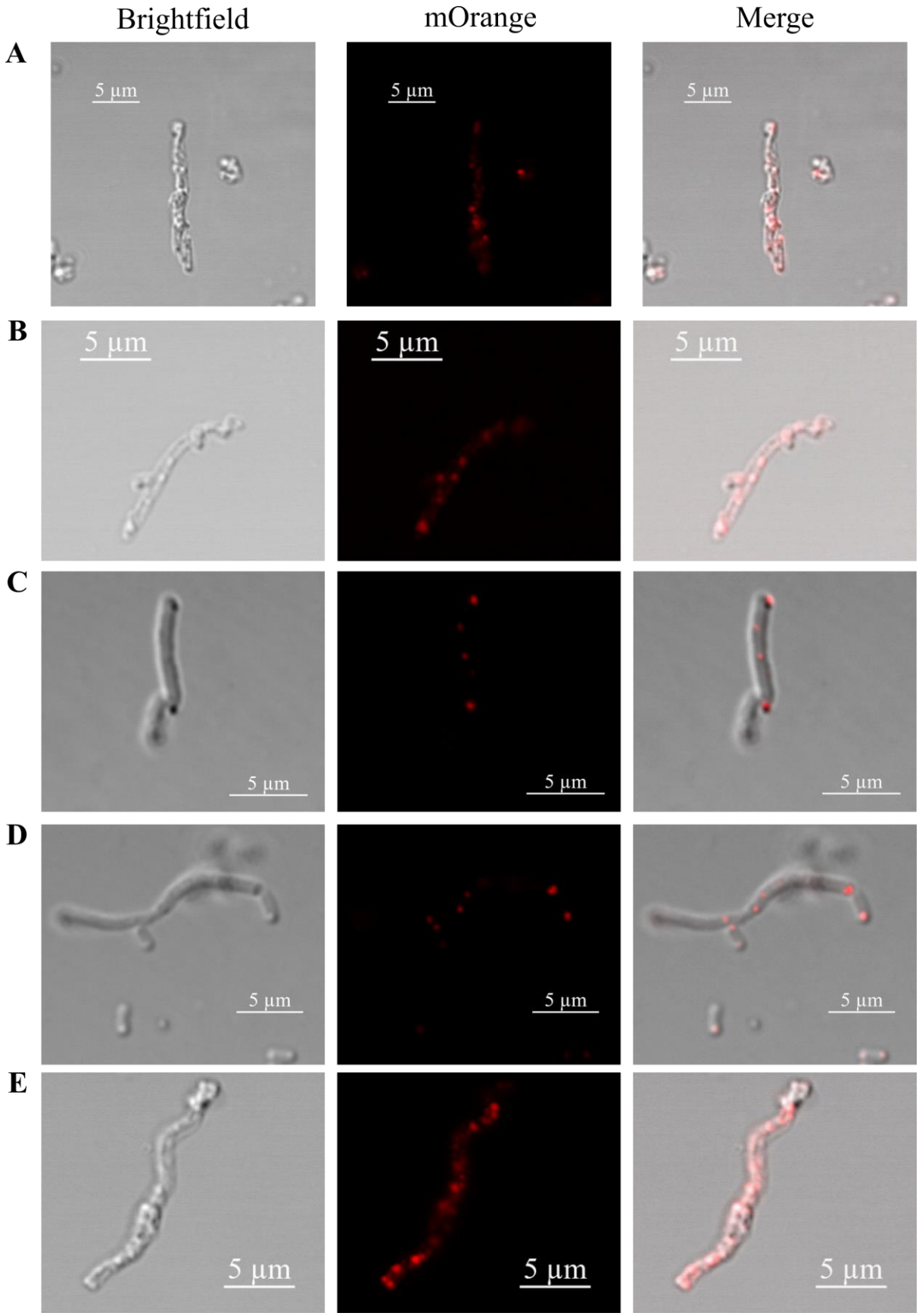

Figure S6 Confocal microscopy of mKO2-tagged Physcomitrella FtsZ2-1 in *E. coli*. BL21 Star™ (DE3) cells transformed with the constructs for mKO2-FtsZ2-1 were induced with 0.5 mM IPTG. Different elongated bacteria were observed (A-E). Scale bars as indicated.

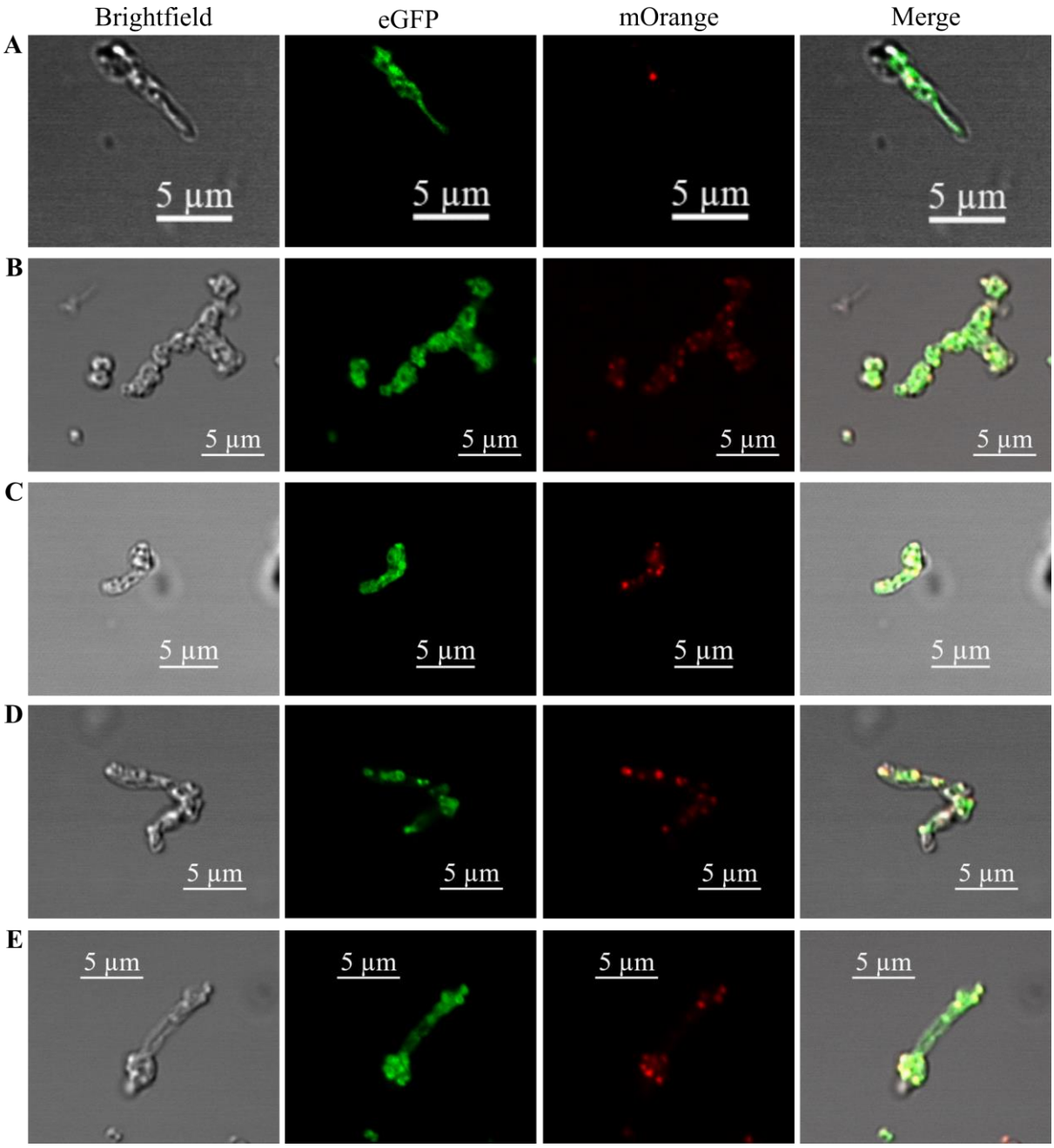

Figure S7 Confocal microscopy of eGFP-tagged Physcomitrella FtsZ1-2 and mKO2-tagged Physcomitrella FtsZ2-1 in *E. coli*.

BL21 Star™ (DE3) cells transformed with the construct for eGFP-FtsZ1-2_mKO2-FtsZ2-1 were induced with 0.5 mM IPTG. Different elongated bacteria were observed (A-E). Scale bars as indicated.

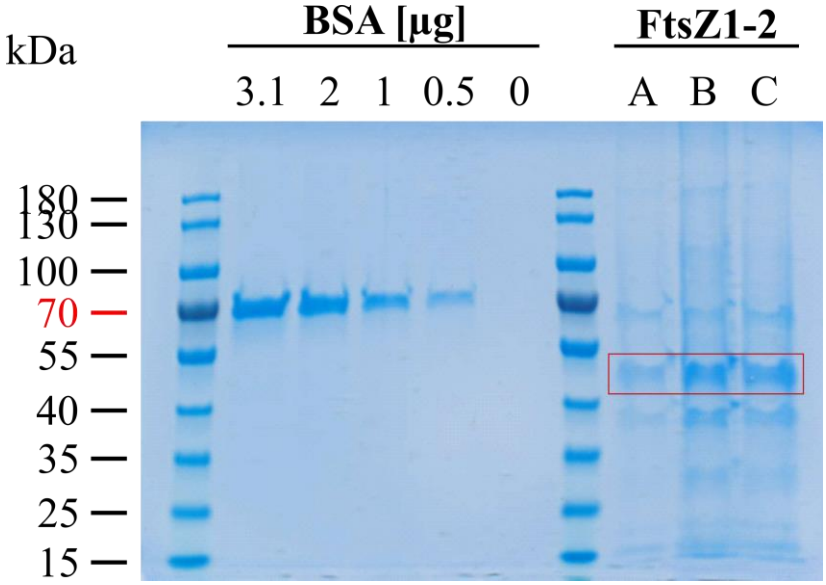

Figure S8: BSA-SDS Gel for quantification of FtsZ1-2.
Purified FtsZ1-2 from different nickel NTA affinity chromatography runs (A, B, C) at 44 kDa. 10 µl of each dialyzed fraction was loaded on the gel, respectively, and the amount of FtsZ1-2 (red rectangle) was calculated via densitometry (GelAnalyzer 19.1; www.gelanalyzer.com). One representative experiment is shown. Ladder: PageRuler™ Prestained Protein Ladder (Thermo Fisher Scientific).

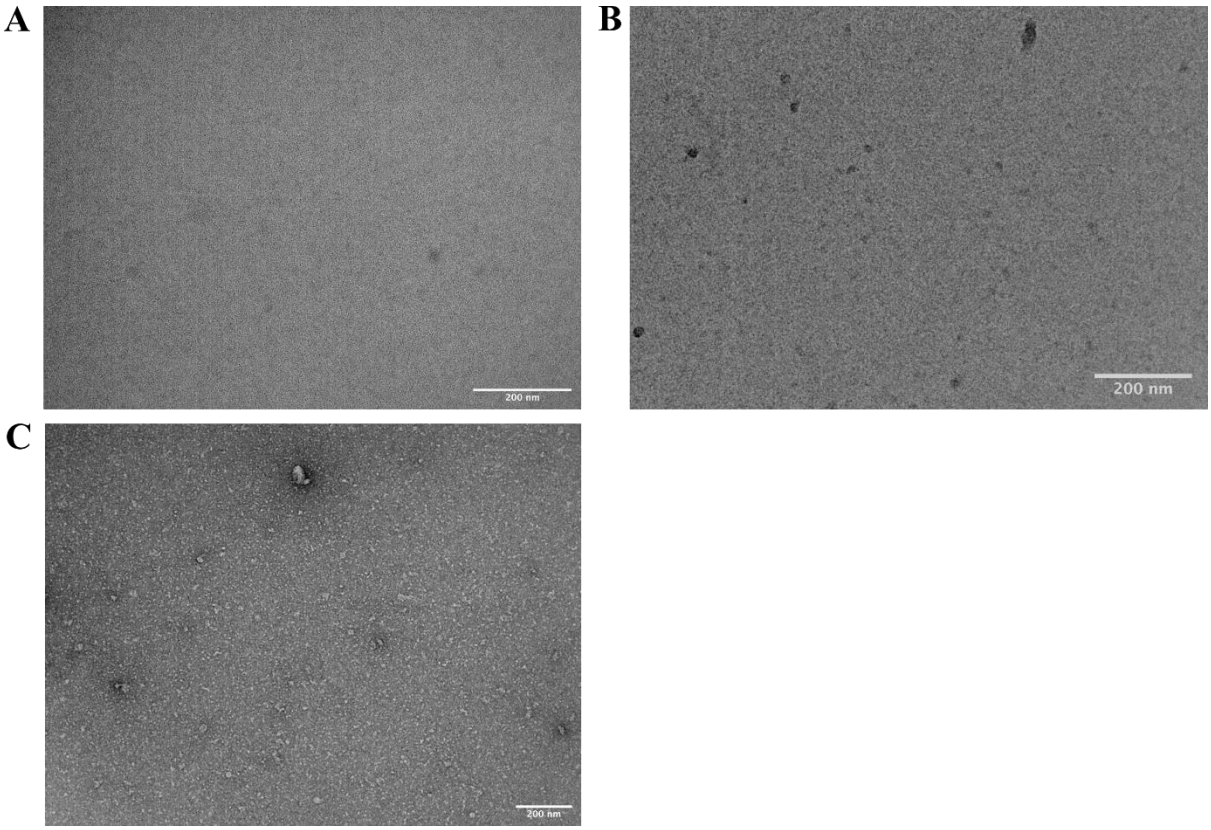

Figure S9 Negative stain transmission electron microscopy of Physcomitrella FtsZ1-2, Physcomitrella FtsZ2-1 together with FtsZ2-1 without GTP as negative control.
15 µM of FtsZ1-2 (A), 15 µM FtsZ2-1 (B) and 7.5 µM FtsZ1-2 mixed with 7.5 µM FtsZ2-1 (C) were incubated at room temperature for 5 min without GTP and then imaged by transmission electron microscopy. Representative images are shown. Scale bars as indicated. Experiments were repeated independently twice with similar results.